

1 Dynamics of environmental conditions during a decline of a *Cymodocea nodosa* meadow

2

3 Mirjana Najdek¹, Marino Korlević¹, Paolo Paliaga², Marsej Markovski¹, Ingrid Ivančić¹,

4 Ljiljana Iveša¹, Igor Felja³ and Gerhard J. Herndl^{4,5}

5 ¹Center for Marine Research, Ruđer Bošković Institute, G. Paliaga 5, 52210 Rovinj, Croatia

6 ²Department of Natural and Health Sciences, University of Pula, Zagrebačka 30, 52100 Pula,
7 Croatia

8 ³Department of Geology, Faculty of Science, University of Zagreb, Horvatovac 102a, 10000
9 Zagreb, Croatia

10 ⁴Limnology and Bio-Oceanography, Center of Functional Ecology, University of Vienna,
11 Althanstrasse 14, 1090 Vienna, Austria

12 ⁵NIOZ, Department of Marine Microbiology and Biogeochemistry, Royal Netherlands
13 Institute for Sea Research, Utrecht University, PO Box 59, Alberta, Den Burg, 1790, The
14 Netherlands

15 *Correspondence to:* Mirjana Najdek (najdek@cim.irb.hr)

16 **Abstract.** The dynamics of the physicochemical and biological parameters were followed
17 during the decline of a *Cymodocea nodosa* meadow in the northern Adriatic Sea from July
18 2017 to October 2018. During the regular growth of *C. nodosa* from July 2017 to March
19 2018, *C. nodosa* successfully adapted to the changes of environmental conditions and
20 prevented H₂S accumulation by its re-oxidation, supplying the sediment with O₂ from the
21 water column and/or leaf photosynthesis. The *C. nodosa* decline was most likely triggered in
22 April 2018 when light availability to the plant was drastically reduced due to increased
23 seawater turbidity that resulted from increased terrigenous input combined with resuspension
24 of sediment and elevated autotrophic biomass. Light reduction impaired photosynthesis of *C.*
25 *nodosa* and the oxidation capability of below-ground tissue. Simultaneously, a depletion of
26 oxygen due to intense oxidation of H₂S occurred in the sediment, thus creating anoxic
27 conditions in most of the rooted areas. These linked negative effects on the plant performance
28 caused an accumulation of H₂S in the sediments of the *C. nodosa* meadow. During the decay
29 of above- and below-ground tissues, culminating in August 2018, high concentrations of H₂S
30 were reached and accumulated in the sediment as well as in bottom waters. The influx of
31 oxygenated waters in September 2018 led to the re-establishment of H₂S oxidation in the
32 sediment and remaining of the below-ground tissue. Our results indicate that if disturbance of
33 environmental conditions, particularly those compromising the light availability, takes place
34 during the recruitment phase of plant growth when metabolic needs are at maximum and
35 stored reserves minimal, a sudden and drastic decline of the seagrass meadow occurs.

36

37 **1 Introduction**

38 Seagrasses are important ecosystem engineers constructing valuable coastal habitats which
39 play a key role in the preservation of marine biodiversity and carbon sequestration (Duarte et
40 al., 2013; Samper-Villareal et al., 2016). Seagrasses extend their active metabolic surfaces
41 (i.e., leaves, rhizomes and roots) into the water column and in the sediment, where root
42 activity might modify the chemical conditions (Marbà and Duarte, 2001). Their canopies and
43 dense meadows are responsible for trapping substantial amounts of sediment particles and
44 organic matter, enhancing water transparency and sediment stability with the dense network
45 formed by the rhizome (Gacia and Duarte, 2001; Hendriks et al., 2008; Widdows et al., 2008).
46 Seagrass rhizospheres store organic matter (Pedersen et al., 1997), promote sulfate reduction
47 (Holmer and Nielsen, 1997), release oxygen (Pedersen et al., 1998) and alter sediment redox
48 potential.

49 Seagrasses require some of the highest light levels of any plant worldwide to provide
50 oxygen to roots and rhizomes and support a large amount of non-photosynthetic tissue (Orth
51 et al., 2006). This make seagrasses sensitive to environmental changes, especially those that
52 deteriorate light availability, such as sediment loading, eutrophication or epiphyte cover on
53 seagrass leaves (Terrados et al., 1998; Halun et al., 2002; Brodersen et al., 2015; Costa et al.,
54 2015). Seagrasses have adapted to a highly variable light environment providing tolerance to
55 short-term periods of low light conditions by balancing carbon supply and respiratory
56 requirements. In a healthy growing population this balance is achieved by increasing the
57 photosynthetic activity, re-allocation of carbohydrate reserves from rhizomes and slowing
58 down growth rates (Collier et al., 2009). Beside metabolic and physiological changes, stress
59 responses under poor light conditions include shedding of leaves and shoots and production of
60 new, altered tissue. At sub-lethal light levels, these changes may be permanent. Below these
61 species-specific minimum light requirements seagrass populations are dying off (Collier et al.,
62 2012). Membrane lipids, particularly polyunsaturated fatty acids (PUFA), as the most
63 responsive constituents have a major role in the adaptation processes of primary producers to
64 fluctuating environmental factors, such as temperature, irradiance or salinity (Viso et al.,
65 1993; Lee et al., 2007; Schmid et al., 2014; Sousa et al., 2017; Beca-Carretero et al., 2018;
66 Beca-Carretero et al., 2019). The changes in the unsaturation degree (UND) of membrane
67 fatty acids affect the maintenance of membrane functions and its resistance to cold stress or

68 poor light conditions. UND depends mostly on the variation of α -linolenic (C18:3n-3, ALA)
69 and linoleic (C18:2n-6, LA), the major unsaturated fatty acids in leaves, implicated in the
70 evolution of oxygen during photosynthesis. LA and ALA are derived from oleic acid by
71 desaturation in the chloroplast and this conversion considerably declines in the dark, being
72 completely inhibited by anaerobiosis (Harris and James, 1965).

73 Sediments inhabited by seagrasses are usually anoxic, highly reduced and rich in sulfide
74 (H_2S), a strong phytotoxin (Koch and Erskine, 2001) which has been implicated in several
75 die-off events of seagrasses (Carlson et al., 1994; Borum et al., 2005; Krause-Jensen et al.,
76 2011). H_2S is produced by sulfate-reducing bacteria that use sulfate as a terminal electron
77 acceptor for the mineralization of organic matter (Jørgensen, 1977; Capone and Kiene, 1988,
78 Canfield et al., 1993). High H_2S concentrations may occur as a consequence of enhanced
79 mineralization due to increased temperature, organic loading or oxygen depletion (Moeslund
80 et al., 1994; Pérez et al., 2007; Mascaró et al., 2009). Under these conditions, sulfides may
81 intrude into plant. Re-oxidation of H_2S in the rhizosphere by incorporation of S^0 in the below-
82 ground tissue has been recognized as a major survival strategy of seagrasses in sulfidic
83 sediments (Pedersen et al., 2004; Holmer et al., 2005; Hasler-Sheetal and Holmer, 2015).
84 Generally, the synergistic effect of oxygen depletion and other stresses, such as sulfide
85 toxicity may shorten the survival of benthic communities and possibly accelerate mortality
86 events (Vaquer-Sunyer and Duarte, 2010).

87 The seagrass *Cymodocea nodosa* (Ucria) Ascherson is widely distributed and common
88 species throughout the Mediterranean (Terrados and Ros 1992; Pedersen et al., 1997;
89 Cancemi et al., 2002; Agostini et al., 2003). For the northern Adriatic, however, only sparse
90 data are available on the standing crop, seasonal dynamics or natural/anthropogenic pressures
91 supporting the ecological or conservation status of *C. nodosa* meadows (Zavodnik et al.,
92 1998; Orlando-Bonaca et al., 2015; 2016). Although *C. nodosa* show large phenotypic
93 plasticity adapting to diverse natural and anthropogenic stressors by physiological and
94 morphological adaptations, a severe decline has been reported during the last decades in
95 coastal areas (Orth et al., 2006; Short et al., 2011; Tuya et al., 2002; 2014), including the
96 northern Adriatic (Orlando-Bonaca et al., 2015; 2019). One of these declines was documented
97 in our study performed from July 2017 to October 2018 in Saline Bay (northern Adriatic Sea).
98 A series of monthly physicochemical and biological measurements were conducted in *C.*
99 *nodosa* tissues, sediment underlying the *C. nodosa* meadow, non-vegetated sediments and

100 surrounding water to i) determine the link between ambient seawater and sediment
101 environmental factors influencing the growth of *C. nodosa*, ii) document the response of *C.*
102 *nodosa* to the changes in environmental conditions that led to the meadow decline and iii)
103 evaluate the conditions leading to the decline of *C. nodosa*.

104 **2 Materials and methods**

105 2.1 Study site

106 Saline Bay is located 4 km northwest of Rovinj (Croatia) at the coast of the northern Adriatic
107 Sea (45°7'5"N; 13°37'20"E, Fig. S1). The bay represents the terminal shallow part of an 800
108 m long inlet, open towards the northwest. The southeastern coast of Saline Bay is
109 characterized by relatively pristine conditions, while the northwestern littoral part has been
110 completely modified by the excavation of coastal mud and the addition of large amounts of
111 gravel to create an artificial beach. Large amounts of silty red soil (*terra rossa*) can be found
112 in the south eastern inner part of the bay in a large muddy flatland which is slowly being
113 eroded by the sea and rain weathering. The main input of freshwater to the bay represents land
114 drainage canals since the year 2017. Even though Saline Bay is protected from the prevailing
115 winds (from the NE and SE) circulations from the northwestern quadrant can occasionally
116 trigger bigger waves resuspending the surface sediments and giving the waters a muddy
117 appearance. At the beginning of this study, the seafloor was covered with large *C. nodosa*
118 meadows spreading from the southwestern coastal area (1.5 m depth) toward the central part
119 of the bay (4 m depth), while at the end of the study only a few small patches persisted in tiny
120 stripes along the shoreline.

121

122 2.2 Sampling

123 The sampling was performed for 15 months from July 2017 to October 2018. Seawater for
124 analyses of nutrients, chlorophyll *a* (Chl *a*), particulate matter concentration and prokaryotic
125 abundance was sampled using plastic containers (10 L). *C. nodosa* (3 – 4 m of depth) was
126 collected together with rhizomes, roots and epiphytic macroalgae by divers using the quadrat
127 sampling method. Three quadrats (20 x 20 cm) were randomly scattered in positions of
128 maximum seagrass coverage (e.g. 100 %). Sediment samples were collected inside vegetated
129 and non-vegetated sediment by divers using plastic core samplers (15 cm, 15.9 cm²). For
130 granulometric composition, organic matter, prokaryotic abundance, total lipids and fatty acid
131 analyses, the cores were cut into 1 cm sections to a depth of 8 cm and lyophilized, except of

132 sections for prokaryotic abundance analysis, that were weighted (approx. 2 g) and fixed with
133 formaldehyde (final conc. 4% v/v) immediately after slicing the sediment core.

134

135 2.3 Temperature (T) and salinity (S) measurements

136 T was measured continuously (in 30 min. intervals) using HOBO pendant temp/light Data
137 Loggers (Onset, USA) which were replaced at each sampling. S was measured on sampling
138 dates by a pIONneer 65 probe (Radiometer analytical, Copenhagen).

139

140 2.4 Inorganic nutrients, Chl *a* and particulate matter (PM) analysis

141 Seawater for all analysis was filtered through combusted Whatman GF/F filters. Nitrate
142 (NO₃), nitrite (NO₂), ammonia (NH₄), phosphate (PO₄) and silicate (SiO₄) were analyzed
143 spectrophotometrically according to Strickland and Parsons (1972). Chl *a* was determined on
144 filters by the fluorometric procedure after extraction in 90 % acetone (Holm-Hansen et al.,
145 1965). PM was determined gravimetrically after filtering up to 5L seawater on pre-weighed,
146 filters which were dried (at 60°C) and reweighed.

147

148 2.5 Determining prokaryotic abundance

149 For determining the prokaryotic abundance in seawater, 2 ml of formaldehyde (final conc. 4%
150 v/v) fixed samples were stained with 4,6-diamidino-2-phenylindol (DAPI, 1 µg mL⁻¹ final
151 conc.) for 10 min (Porter and Feig, 1980). In sediment samples, prokaryotes were detached
152 from the sediment particles by addition of Tween 80 (0.05 mL) and ultrasonicated for 15 min
153 (Epstein and Rossel, 1995). After sonication, 1 mL of the supernatant was stained with DAPI
154 (final conc. 5 µg/mL). DAPI stained samples were filtered onto black polycarbonate filters
155 (Whatman, Nuclepore, 0.22 µm) and counted under an epifluorescence microscope (Zeiss
156 Axio Imager Z1).

157

158 2.6 Biometry of *C. nodosa* and epiphytic macroalgae

159 The material from each quadrat was washed under running seawater to remove sediment.
160 From each quadrat algae, leaves and rhizomes with roots were separated. The length of the
161 longest leaf on each shoot was measured and the shoots were counted. Species of macroalgae
162 were determined, and their coverage was estimated according to the Braun-Blanquet scale.

163 Separated samples were washed with filtered and autoclaved seawater, weighed, dried at 60
164 °C for 48 h and re-weighed. The dry mass was calculated per area (g m^{-2}).

165

166 2.7 Granulometric composition of the sediment and its organic matter content

167 For granulometric analysis of the sediment, each sample was wet sieved through a set of
168 seven standard ASTM sieves (4-, 2-, 1-, 0.5-, 0.25-, 0.125-, 0.063-mm mesh size). The
169 fraction that passed through the 0.063-mm sieve was collected and analyzed following the
170 standard sedigraph procedure (Micromeritics, 2002). The material that was retained on the
171 sieves was dried and weighted. The data obtained by both techniques were merged to obtain a
172 continuous grain size range and analyzed with the statistic package Gradistat v 6.0. Sediments
173 were classified according to Folk (1954). The sediment permeability was calculated based on
174 median grain size (d_g) following the empirical relation by Gangi (1985). The organic matter
175 content was determined as ignition loss after heating dried sediment sections at 450°C for 4 h
176 in a muffle furnace.

177

178 2.8 Oxygen (O_2), hydrogen sulfide (H_2S) and redox potential (Eh) profiling

179 The microprofiles of O_2 , H_2S and Eh were measured on intact cores immediately after
180 sampling using a motorized micromanipulator (MMS9083) equipped with microsensors OX-
181 100 and H_2S -200, redox microelectrode RD-200 coupled with reference electrode REF-RM
182 (Unisense A/S, Denmark). Prior to the measurements, the OX-100 microsensor was calibrated
183 using a two-point oxic – anoxic calibration; H_2S -200 was calibrated in fresh Na_2S solutions
184 using eight-point calibration ($1\mu\text{M}$ - $300\mu\text{M}$ in a de-oxygenated calibration buffer
185 (NaAc/HAc , $\text{pH} < 4$); RD-200 with REF-RM was calibrated using two point calibration by
186 simultaneous immersion of electrodes in quinhydrone redox buffers prepared in pH 4 and pH
187 7 buffers, all according to the manufacturer's recommendation. During measurements,
188 sediment cores were placed in a pool filled with seawater from the sampling site to maintain
189 *in situ* temperature. From July to October 2017 H_2S was measured spectrophotometrically in
190 pore waters (Cline, 1969) squeezed out by centrifugation from each section (5 mm) of the
191 sediment cores.

192

193 2.9 Total lipids, fatty acid composition and elemental sulfur (S^0)

194 Lyophilized samples of seagrass tissues, macroalgae, sediment or particulate matter were
195 weighed and extracted into a solvent mixture of dichloromethane/methanol (DCM: MeOH,
196 2:1) in an ultrasonic bath at 35°C with three solvent mixture changes. The extracts were
197 pooled and separated into layers by addition of 0.9% NaCl solution. Lower DCM layers
198 (containing lipids) were released over Na₂SO₄ anhydride, collected in pre-weighed round
199 bottom flasks and evaporated to dryness using rotavapor. After evaporation, flasks were re-
200 weighed, and total lipid concentrations (TL, mg g⁻¹ DW) were calculated from the difference
201 in weight. For fatty acids determination, lipid extracts were saponified (1.2 M NaOH in
202 methanol), acidified (6 M HCl), methylated (14% BF₃ in methanol) and extracted into DCM.

203 Fatty acid methyl esters (FAME) were analyzed by Agilent gas-liquid chromatography
204 (GLC) 6890 N GC System equipped with a 5973 Network Mass Selective Detector, capillary
205 column (30 m x 0.3 mm x 0.25 μm; cross-linked 5 % phenylmethylsiloxane) and ultra-high
206 purity helium as the carrier gas. The GLC settings were as follows: programmed column
207 temperature rise from 145°C by 4°C/min to 215°C, then by 1°C/min to 225°C and finally by
208 4°C/min to 270°C at constant column pressure of 2.17 kPa. Retention times, peak areas and
209 mass spectra were recorded on the ChemStation Software. FAME were identified by mass
210 spectral data and family plots of an equivalent chain length (ECL) for GC standards. Applied
211 GC standards were: FAME mix C18–C20, PUFA1, PUFA3 standards (Supelco/Sigma-
212 Aldrich, Bellefonte, PA, USA); C4–C24 FAME standard mix, cod liver oil and various
213 individual pure standards (Sigma, Neustadt, Germany).

214 The following indices of fatty acid profiles were calculated: saturated fatty acids (SAT),
215 monounsaturated fatty acids (MUFA), polyunsaturated fatty acids (PUFA) and the
216 unsaturation degree (UND). UND was employed to evaluate the degree of organic matter
217 degradation due to more susceptibility of unsaturated, particularly polyunsaturated,
218 components to degradation and calculated according to the formula
219 $[1*(\% \text{ mono-})+2*(\% \text{ di-})+3*(\% \text{ tri-})+4*(\% \text{ tetra-})+5*(\% \text{ penta-})+6*(\% \text{ hexa-enoic})]/\% \text{ SAT}$
220 (Pirini et al., 2007). To evaluate the input of terrestrial organic matter relative to that of
221 marine origin in particulate matter, the terrestrial to aquatic acid ratio (TAR= C24+C26+C28 /
222 C12+C14+C16) was used (Cranwell et al., 1987; Bourbonniere and Meyers, 1996).

223 In FAME chromatograms elemental sulfur (S⁰), eluted as S₈ (m/z 256), was identified by
224 comparison of retention time and characteristic fragment ions in samples and standard
225 solutions. The concentration of S⁰ was estimated on the base of the calibration curve prepared

226 for standard solution of S₈ (Aldrich, Germany) in cyclohexane (2-20 mg L⁻¹). The calibration
227 curve was determined under the same GLC settings as FAME. Limit of detection (LoD) and
228 limit of quantitation (LoQ) were calculated from the parameters of the calibration curve
229 constructed on the basis of the 3 lowest concentrations in 3 replicates. LoD and LoQ (0.92 mg
230 L⁻¹ and 2.80 mg L⁻¹, respectively) were more than twice the values obtained by Rogowska et
231 al. (2016) probably due to higher injector and column temperature used in this study than they
232 proposed as optimal for S determination.

233

234 2.10 Data analyses

235 A multivariate analysis, hierarchical clustering and K-means methods (Systat 12) was applied
236 to group *C. nodosa* above- and below-ground tissues according to the similarity of their fatty
237 acid profiles and indices, i.e., physiological condition during the investigated period.

238 Sediment data were analyzed for two groups of sediment layers, the upper layer (0- 4 cm)
239 where most of rhizomes and roots are located, and the lower layers (5-7 cm). Differences
240 between vegetated and non-vegetated sediment samples in each sediment layer were tested by
241 one-way ANOVA. Correlations among parameters were tested using the Pearson's correlation
242 coefficient (r). The level of statistical significance was $p < 0.05$. A multivariate principal
243 component analysis (PCA, Primer 6) was applied to identify the most important variables
244 explaining differences between vegetated and non-vegetated sediments. Correlation matrices
245 were constructed using variables: H₂S, Eh, O₂, S⁰, PA, TL and UND. All variables were
246 normalized due to their different scales. Only the principal components with eigenvalues >1
247 were considered.

248

249 **3 Results**

250 3.1 Water column

251 3.1.1 Environmental variables

252 During summer of 2017 daily means of sea-bottom temperature in *C. nodosa* meadow ranged
253 between 26°C and 28°C. During autumn seawater temperatures decreased below 12°C until
254 the end of December. The coldest period was recorded at the beginning of March lasting only
255 for a few days (min. 8.62°C). From April to mid-July 2018, temperature increased with
256 moderate fluctuations to the maximum of 29.26°C recorded in August 2018 (Fig. 1a).

257 Concentrations of inorganic nutrients and Chl *a* were generally low. The highest
258 concentrations (DIN: 8.27 μM ; PO_4 : 0.18 μM ; SiO_4 : 9.82 μM ; Chl *a*: 0.89 $\mu\text{g L}^{-1}$) associated
259 with the lowest salinity (34.2) were found in September 2017 (Table S1). The abundance of
260 prokaryotes ($2.6\text{-}11.3 \times 10^5 \text{ cell mL}^{-1}$) varied seasonally and significantly correlated to
261 seawater temperatures ($r = 0.618$; $p < 0.05$). In contrast, salinity (S: 34.2 - 38.5) and
262 concentrations of particulate matter (PM: 3.84 - 14.21 mg L^{-1}) showed irregular variations
263 (Fig. 1b) and a significant opposite trend ($r = -0.630$; $p < 0.05$).

264 The particulate lipids exhibited the highest unsaturation degree (UND) during
265 summer/early autumn 2017 and small increases of UND in April and September/October
266 2018 (Fig. 1c). UND was significantly correlated with Chl *a* ($r = 0.603$; $p < 0.05$). In contrast,
267 terrestrial to aquatic ratio (TAR) considerably increased in April and was the highest in
268 August 2018 (Fig. 1c). TAR was negatively correlated to UND ($r = -0.644$, $p < 0.05$) and
269 positively to particulate matter ($r = 0.641$, $p < 0.05$). Although PUFA with 18 C atoms made
270 the largest contribution to the total PUFA pool, C20 PUFA, mainly of phytoplankton origin,
271 showed a similar trend as observed for UND (Fig. S2, Table S2).

272

273 3.2 *Cymodocea nodosa* meadow

274 3.2.1 Biometry

275 *C. nodosa* leaves and shoots reached the highest biomass ($285.3 \pm 57.4 \text{ g m}^{-2}$), length ($102.4 \pm$
276 26.6 mm) and shoot density ($3703 \pm 334 \text{ shoots m}^{-2}$) in October 2017 (Fig. 2a). After the
277 appearance of the regular vegetation minimum in November 2017, biometric indices further
278 decreased reflecting the decay of the meadow in summer 2018. In August 2018, only yellow
279 to brownish leaves on sparse shoots were collected ($4.5 \pm 1.3 \text{ g m}^{-2}$, $5.4 \pm 1.3 \text{ mm}$ and 30 ± 35
280 shoots m^{-2}). In September and October 2018, no shoots or leaves were observed (Fig. 2a). The
281 biomass of rhizomes and roots reached also its maximum in October 2017 ($599.7 \pm 36.8 \text{ g m}^{-2}$).
282 In contrast to leaves and shoots, the belowground biomass was stable until March 2018
283 when a decline was observed that continued until October 2018 ($30.5 \pm 6.8 \text{ g m}^{-2}$) (Fig. 2a).

284

285 3.2.2 Total lipid (TL) concentrations and fatty acid composition

286 TL in the *C. nodosa* above-ground tissue ($6.7 - 25.3 \pm 2.4 \text{ mg g}^{-1} \text{ DW}$) increased until
287 February 2018, when maximum TL concentrations were measured (Fig. 2b). Thereafter, TL
288 concentrations decreased until August 2018. During this period, the belowground TL

289 concentration ($6.3 \pm 1.9 - 15.9 \pm 1.1 \text{ mg g}^{-1} \text{ DW}$) was generally lower than the above-ground
290 TL concentrations and the trend was similar to that of leaves. The minimum concentrations of
291 TL were observed in September 2018, while in October 2018, concentrations similar to that
292 measured in October 2017 were observed (Fig. 2b).

293 The major fatty acid components in *C. nodosa* tissues were palmitic (C16:0) amongst the
294 saturated (SAT) and oleic (C18:1n-9) in monounsaturated fatty acids (MUFA). In the above-
295 ground tissue, the main polyunsaturated fatty acids (PUFA) were α -linolenic (C18:3 n-3,
296 ALA) and linoleic (C18:2 n-6, LA), while in the belowground tissue LA was dominant (Fig.
297 2b). The dynamics of UND in the above-ground tissue was principally influenced by changes
298 in ALA and LA. LA/ALA ratios were < 1 from July 2017 to March 2018, and > 1 from April
299 to July 2018 (Fig. 2b). In August 2018, the LA/ALA ratio was infinite due to the absence of
300 ALA (Fig. 2b). Elemental sulfur (S^0) was detected only in decaying leaves in August 2018
301 ($0.21 \text{ mg g}^{-1} \text{ DW}$). In the belowground tissue, S^0 was detected in all samples (Fig. 2b). Higher
302 concentrations were measured during summer 2017 (up to $0.39 \pm 0.06 \text{ mg g}^{-1} \text{ DW}$). S^0
303 increased from minimum concentrations in April ($0.02 \pm 0.01 \text{ mg g}^{-1} \text{ DW}$) until September
304 2018 reaching $1.42 \text{ mg g}^{-1} \text{ DW}$ (Fig. 2b).

305 According to the fatty acid profiles, *C. nodosa* leaves were classified in three groups,
306 except for the leaves collected in August 2018 (Fig. 3). The most distinguishing features
307 specifying physiological differences between Group 1 (July - October 2017 and February -
308 March 2018), Group 2 (November - December 2017 and April - May 2018) and Group 3
309 (June and July 2018) were decreasing mean values of PUFA, UND, ALA and LA and
310 increasing means of SAT and the proportion of long-chain saturated fatty acids ($C \geq 24$). In
311 the ungrouped leaves from August 2018 ALA was not found, PUFA and UND were at a
312 minimum, while SAT and $C \geq 24$ at a maximum (Table S3). Three groups of rhizomes and
313 roots (Group 1: July - October 2017 and February - March 2018; Group 2: November -
314 December 2017 and April - May 2018 and Group 3: (June - October 2018) showed similar
315 characteristics to the groups 1, 2 and 3 of related leaves (Table S4).

316

317 3.2.3 Epiphytic macroalgae

318 From July 2017 to February 2018 different taxa of macroalgae belonging to the three phyla
319 Chlorophyta (*Halimeda tuna*, *Dasycladus vermicularis*, *Cladophora prolifera*, *Udotea*
320 *petiolata*), Rhodophyta (*Rytiphlaea tinctoria*, *Peyssonnelia* spp, *Gelidium* sp.) and

321 Ochrophyta (*Dictyota dichotoma*) were covering the meadow in varying proportions and
322 abundances (Fig. 4). After March 2018, when only few individuals of *Peyssonnelia* sp. were
323 found, macroalgae were no longer present in the *C. nodosa* meadow.

324 Although the fatty acid profiles of macroalgal communities were highly variable, the
325 contribution of 18- and 20 PUFA to the total PUFA pool generally depended on the prevailing
326 phyla and their characteristic PUFA pattern. The algae belonging to Rhodophyta and
327 Ochrophyta are richer in 20 PUFA (C20:5n-3, C20:4n-6), while Chlorophyta are generally
328 showing prevalence of 18 PUFA (C18:3n-3, C18:2n-6) (Schmid et al., 2014, Gao et al.,
329 2018). Furthermore, their contribution to biomass varied due to large differences in
330 morphology, which most likely also contributed to the variability of fatty acid profiles. 18
331 PUFA and 20 PUFA showed the highest contribution to the total PUFA pool during the
332 dominance of Chlorophyta and Rhodophyta in the macroalgal community, respectively. In
333 most samples, the lowest contribution to the total PUFA pool was observed for 16 PUFA and
334 22 PUFA (Fig. S3).

335

336 3.3 Sediment

337 3.3.1 Granulometric composition

338 According to the granulometric composition, median grain sizes (d_g) and permeability (k) the
339 vegetated and non-vegetated sediments were classified as slightly gravelly sandy mud (g)sM,
340 fine grained ($d_g < 165 \mu\text{m}$) and low permeable to impermeable sediment ($k < 2 \cdot 10^{-11} \text{ m}^2$). In
341 general, the *C. nodosa* sediment consisted of a significantly higher proportion of sand (Sa),
342 and lower proportion of silt (Si) and clay (C) (Sa, $41.11 \pm 4.34 \%$; Si, $46.44 \pm 2.86 \%$; C, 9.63
343 $\pm 2.76 \%$) in comparison to non-vegetated sediment (Sa, $20.53 \pm 10.49 \%$; Si, $53.24 \pm 6.76 \%$;
344 C, $23.29 \pm 4.86 \%$). The median grain size and permeability in *C. nodosa* sediment (d_g , 37.51
345 $\pm 17.97 \mu\text{m}$, k , $1.22 \cdot 10^{-12} \pm 1.13 \cdot 10^{-12} \text{ m}^2$) were significantly higher than in non-vegetated
346 sediment (d_g , $10.86 \pm 5.34 \mu\text{m}$; k , $1.04 \cdot 10^{-13} \pm 1.02 \cdot 10^{-13} \text{ m}^2$). The upper layers of both cores
347 (0 - 4 cm) had larger particles, while the lower layers (5 - 8 cm) showed a uniform distribution
348 of smaller grain sizes (Fig. 5).

349

350 3.3.2 O_2 , E_h , H_2S and S^0

351 Oxygen concentrations (O_2) in the bottom water of the *C. nodosa* meadow varied in a wide
352 range ($0 \mu\text{M} - 171.4 \pm 17.6 \mu\text{M}$) and generally followed the O_2 saturation trend (Fig. 6a).

353 From May to June 2018, O₂ decreased below 62.5 μM, considered as severe hypoxia (Vaquer-
354 Sunyer and Duarte 2008) and was completely depleted in July 2018 (Fig. 6a). From August to
355 October 2018, O₂ increased again. The variations of O₂ in the bottom water of the non-
356 vegetated sediment were similar to those in the *C. nodosa* meadow albeit generally higher
357 (79.4 ± 10.4 μM – 212.2 ± 33.4 μM) than in the vegetated sediment except for September and
358 October 2018 (Fig. 6a).

359 In general, O₂ penetration depth in the vegetated and non-vegetated sediment co-varied
360 with the O₂ concentration in the bottom layer, penetrating deeper when its concentration in the
361 bottom water was higher (Fig. 6b). In the vegetated sediment, O₂ was mainly depleted down
362 to 1 cm of depth. In the non-vegetated sediment, the oxygen penetration depth was up to 4
363 times higher than in vegetated sediments, except for the period from August 2018 to October
364 2018 when the penetration depths were similar (Fig. 6b).

365 The thickness of the oxic (Eh > 150 mV) and suboxic (150 mV > Eh > 0 mV) layers in the
366 vegetated sediment increased from July 2017 (~ 0.5 cm) to March 2018 (~ 4 cm), and
367 decreased progressively from April (~ 0.8 cm) towards the surface in July 2018, when the
368 entire sediment core was anoxic (Eh < 0). From August (~ 1 cm) to October 2018 (~ 2.5 cm)
369 the oxic and suboxic layer thickness increased again (Fig. 7). Oxic conditions (Eh > 0)
370 generally reflected O₂ concentrations in the bottom waters. The dynamics of Eh in non-
371 vegetated sediment were similar to those in the vegetated sediment. However, the thickness of
372 the oxic layer was considerably larger than in the vegetated sediment. Reducing conditions
373 (Eh < 0) were only recorded in July and August 2017 (Fig. 7).

374 Concentrations of free H₂S in the pore water of the vegetated sediment generally increased
375 with depth creating an accumulation zone mainly within the upper sediment layers (1 - 4 cm)
376 (Fig. 7). From July to November 2017, H₂S concentrations increased up to 120 μM (at 4 - 5
377 cm). In December 2017, H₂S was low and uniformly distributed throughout the core (< 5
378 μM). H₂S concentrations increased and the accumulation layer was ascending from March (up
379 to 34.2 ± 12.8 μM; 5 - 7 cm) to April 2018 (up to 177.2 ± 125.1 μM; 3.5 - 4.5 cm). During
380 May 2018 (up to 107.8 ± 75.9 μM; 2.5 - 4 cm), June (up to 199.0 ± 6.3 μM; 1.5 - 6 cm) and
381 July (up to 210.1 ± 138.9 μM; bottom water - 6 cm) a propagation of the accumulation zone
382 was observed in addition to an increase in H₂S (Fig. 7). In August 2018 (up to 1164.1 ± 702.1
383 μM; bottom water - 7 cm) extremely high concentrations over the entire sediment core were
384 recorded. In September and October 2018, H₂S concentrations decreased (down to 140.0 ±

385 25.3 and $72.7 \pm 52.7 \mu\text{M}$; bottom water - 7 cm and 1 - 7 cm, respectively). In the non-
386 vegetated sediment, H_2S depth profiles were similar to those in vegetated sediments, but the
387 concentrations were generally lower, except for the summer of 2017 when the concentrations
388 were comparable but the accumulation zones deeper (Fig. 7).

389 S^0 mainly occurred in oxic ($\text{Eh} > 150 \text{ mV}$) and suboxic ($150 \text{ mV} > \text{Eh} > 0 \text{ mV}$) layers of
390 both, vegetated and non-vegetated sediments (Fig. 7). Generally, the ranges of approximated
391 S^0 concentrations in vegetated sediment ($8.5 \cdot 10^{-5} - 0.39 \text{ mg} \cdot \text{g}^{-1} \text{ DW} \sim 2.6 \cdot 10^{-3} - 12.1 \mu\text{mol} \cdot \text{g}^{-1}$
392 DW), except for the extreme value in April 2018 ($0.99 \text{ mg} \cdot \text{g}^{-1} \text{ DW} \sim 30.8 \mu\text{mol} \cdot \text{g}^{-1} \text{ DW}$),
393 were similar to those found at the non-vegetated sites ($2.9 \cdot 10^{-4} - 0.28 \text{ mg} \cdot \text{g}^{-1} \text{ DW} \sim 9.2 \cdot 10^{-3} -$
394 $8.9 \mu\text{mol} \cdot \text{g}^{-1} \text{ DW}$).

395

396 3.3.3 Prokaryotic abundance

397 Prokaryotic abundance varied largely in vegetated ($2.1 - 39.9 \cdot 10^7 \text{ cells g}^{-1}$ fresh weight, FW)
398 and non-vegetated sediments ($3.7 - 24.1 \cdot 10^7 \text{ cells g}^{-1}$ FW). Prokaryotic abundance was
399 significantly higher in the upper than the lower layers of vegetated ($F = 40.553, p < 0.05$) and
400 non-vegetated ($F = 52.531, p < 0.05$) sediments (Fig. 8). Prokaryotic abundance showed
401 significant monthly changes in the upper ($F = 3.053, p < 0.05$) and lower layer ($F = 5.035, p <$
402 0.05) of vegetated sediments, in contrast to both layers of non-vegetated sediments ($p > 0.05$).
403 Prokaryotic abundances were significantly higher in the upper layers ($F = 44.577, p < 0.05$)
404 and significantly lower in the lower layers ($F = 5.986, p < 0.05$) of vegetated than in the
405 respective layers of non-vegetated sediments (Fig. 8). In the upper sediment layer, prokaryotic
406 abundances were significantly higher in the vegetated than in the non-vegetated sediments
407 from July to October 2017 and from June to August 2018 (Fig. 8). In the lower layers of
408 vegetated sediments, prokaryotic abundance was significantly higher than in the non-
409 vegetated sediments in October 2017 and in August and September 2018 (Fig. 8).

410

411 3.3.4 Organic matter, total lipids and fatty acid composition

412 The concentrations of organic matter (OM) and total lipids (TL) were highly correlated in
413 vegetated (OM: $37.6 - 231.1 \text{ mg/g DW}$, TL: $0.15 - 2.75 \text{ mg/g DW}$; $F = 214.172, p < 0.05$) as
414 well as in non-vegetated sediments (OM: $56.7 - 160.3 \text{ mg/g DW}$, TL: $0.33 - 2.39 \text{ mg/g DW}$; F
415 $= 45.569, p < 0.05$). OM and TL generally decreased with depth and exhibited similar

416 changes throughout the investigated period with significantly higher concentrations in upper
417 than in lower sediment layers ($p < 0.05$) (Fig. 9).

418 In the vegetated sediment, TL showed significant monthly changes in the upper ($F =$
419 11.418 , $p < 0.05$) and lower sediment layers ($F = 3.186$, $p < 0.05$), in contrast to both layers of
420 non-vegetated sediment ($p > 0.05$). From July to October 2017, in the upper layer of vegetated
421 sediments, TL was significantly higher than in non-vegetated sediments (Fig. 9). From
422 November 2017 onwards, TL decreased slightly until April 2018, reaching similar
423 concentrations as TL in non-vegetated sediments (Fig. 9). TL concentrations decreased
424 markedly in May and continued until August 2018. During that period, TL in vegetated
425 sediments was significantly lower than in non-vegetated sediments. In September and October
426 2018, TL concentrations in vegetated sediments were similar to those in non-vegetated
427 sediment (Fig. 9).

428 The fatty acid composition of vegetated and non-vegetated sediments was similar and in
429 both layers characterized by the prevalence of SAT (vegetated upper: 71.2 - 90.4%, lower:
430 75.9-89.1%; non-vegetated upper: 71.2-80.7%, lower: 78.2-82.5%) over MUFA (vegetated
431 upper: 7.6-22.9%, lower: 9.0-19.9%; non-vegetated upper: 17.8-24.1%, lower: 15.3-18.2%)
432 and PUFA (vegetated upper: 1.9-6.9%, lower: 1.9-5.1%; non-vegetated upper: 1.7-4.8%,
433 lower: 1.7-3.9%). The trends of the monthly changes in UND were similar in both layers of
434 both sediment types. Those variations were less pronounced in the non-vegetated sediment
435 where UND varied in narrower ranges in both layers (upper: 0.26-0.51, lower: 0.23-0.33) than
436 in vegetated sediment (upper: 0.13-0.57, lower: 0.14-0.37). From July to October 2017 and in
437 April 2018, UND was higher in the upper layers of vegetated sediment than in non-vegetated
438 one, while from November 2017 to March 2018, UNDS of both sediments were lower than in
439 previous period (Fig. 9). From June to August 2018, UND decreased considerably in
440 vegetated sediment, being lower than in non-vegetated sediments. During September and
441 October 2018, an increase of UND was observed in both sediments. In the lower layers,
442 UNDS were similar, except for July and August 2018 when a considerable decrease of UND
443 was observed in vegetated sediments (Fig. 9).

444 The proportions of PUFAs with chain lengths of 16, 18, 20, and 22 C atoms within the
445 PUFA pool were similar between the respective layers of both sediments. Throughout the
446 study period, the highest contribution of 18PUFA originated from *C. nodosa* detritus and
447 Chlorophyta was observed (Fig. S4, Table S2). From July to October 2017, April to May

448 2018 and September to October 2018, a contribution of 20PUFA attributed to phytoplankton
449 and Rhodophyta was also detected. 16PUFA and 22PUFA accounted for the smallest
450 contribution to the PUFA pool and were found in seston and macroalgae (Fig. S4, Table S2).
451 The similarities between the sediments were also observed in the contribution of the main
452 SAT components to the SAT pool from July 2017 to March 2018 and from September to
453 October 2018 (Fig. S4, Table S2). From April to August 2018, an increase of the long-chain
454 ($C \geq 24$) and common (C16:0 + C18:0) fatty acids followed by the decrease of bacterial fatty
455 acids (BACT) contribution to the SAT pool was observed in both layers of the vegetated
456 sediment. In contrast, the contribution of these components to the SAT pool was fairly
457 invariable in non-vegetated sediments during the same period (Fig. S4, Table S2).

458

459 3.3.5 Relationship between different physicochemical parameters

460 The relationships between H_2S , O_2 , TL, S^0 , PA, Eh and UND in vegetated and non-vegetated
461 sediment are shown in the principal component analysis, where PC1 explained 42.5 % and
462 PC2 14.4 % of variability (Fig. 10). The loadings for positive relationships were obtained for
463 H_2S (0.298) on PC1 and Eh (0.541) and O_2 (0.327) on PC2. For the negative relationships, the
464 loadings were for TL (-0.534), UND (-0.494), S^0 (-0.388), Eh (-0.327), PA (-0.296) and O_2 (-
465 0.191) on PC1, and H_2S (-0.536), S^0 (-0.485), TL (-0.165) and UND (-0.221) on PC2.

466 PC1 separated most of the upper sediment layers (July 2017 - May 2018, September -
467 October 2018) according to the higher concentrations of TL and S^0 , higher UND and more
468 positive Eh from the most of the lower layers and upper layers of vegetated sediments (June -
469 August 2018) with increased H_2S concentrations. On PC2, the vegetated was separated from
470 the non-vegetated sediment due to higher concentrations of H_2S , S^0 and more negative Eh,
471 which characterized vegetated sediments during almost the entire study period. The extreme
472 concentrations of S^0 and H_2S found in the upper layer in April and the lower layer in August
473 2018, respectively, were responsible for the considerable separation of these layers from all
474 other vegetated layers (Fig. 10).

475

476 4 Discussion

477 Saline Bay is a shallow, highly dynamic coastal area characterized by frequent turbid waters
478 due to the combined effect of land run-off and wind-driven resuspension of fine sediment.
479 Nutrients and Chl a (as a proxy for autotrophic biomass) varied in the ranges characteristic for

480 the oligotrophic coastal waters off Rovinj (Ivančić et al., 2018). The dynamics of particulate
481 matter was associated with freshwater input. The higher contribution from autochthonous
482 sources was observed during the increases of autotrophic biomass. However, only in
483 September 2017, this increase was supported by nutrients from the water column, while all
484 other increases were most likely connected to bottom waters where phytoplankton could have
485 been supplied with nutrients through sediment resuspension. The considerable increase in the
486 particulate matter of terrigenous origin from April to August 2018 suggested the enhanced
487 land run-off in that period.

488 In temperate Mediterranean coastal waters *C. nodosa* meadows show a clear unimodal
489 annual growth cycle, reaching maximum development in summer, and minima during winter
490 and a particularly active growth phase in spring (Terrados and Ross, 1992; Zavodnik et al.,
491 1998; Agostini et al., 2003). In Saline Bay, the maximum biomass was measured in October
492 2017. This shift from summer to early autumn was most likely due to an intense grazing
493 activities (Cebrian et al., 1996; Valentine and Duffy, 2006) suggested by a prevalence of
494 visibly grazed leaves during July and August 2017. A minimum growth occurred during late
495 autumn/winter, as commonly observed. However, during the spring 2018, phenological
496 parameters continued to decrease in spite of established favorable environmental conditions
497 for growth, i.e., increase in water temperature, intensity and period of solar radiation. This
498 decrease continued until the complete extinction of the above-ground tissue in August 2018.
499 The belowground tissue followed a similar trend, but with less expressed changes. Still, their
500 recognizable remnants were found after the loss of the above-ground tissues.

501 Organic matter and closely correlated total lipids in the sediment of *C. nodosa* rooted area
502 changed significantly throughout the investigated period, in contrast to organic matter in non-
503 vegetated sediment. Nevertheless, considerable similarity in the quality and degradation of
504 lipid matter at both, the vegetated and the non-vegetated sites indicates an important
505 contribution of detritus imported from the meadow as a source of organic matter for
506 prokaryotes in non-vegetated sediments. This close coupling could be expected due to site
507 proximity and lower organic content of the non-vegetated sediment, which should enhance the
508 dependence of prokaryotes on the imports of seagrass detritus from the adjacent meadows
509 (Holmer et al., 2004). Significant enrichment of *C. nodosa* sediment with unsaturated, more
510 labile components only during abundant growth of meadow could be explained by more
511 efficient entrapment of seston material within the meadow (Gacia and Duarte, 2001). Such

512 easily utilizable organic matter, including dissolved monomeric carbohydrates, leaching out
513 during decomposition of *C. nodosa* leaves stimulated prokaryotic growth as previously
514 observed (Peduzzi and Herndl, 1991).

515 From July 2017 to March 2018, an adaptation of *C. nodosa* leaves to the decreasing light
516 and temperature occurred. Until October 2017, the temperature of the water column was still
517 optimal for elongation of the leaves and biomass increase, while the ambient light intensities
518 were continuously decreasing. An additional reduction of available light might occur from the
519 self-shading effect due to high canopy biomass, and/or shading due to epiphytic macroalgae
520 growth. Desaturation of low and fairly invariable lipids during the most active growth phase
521 suggested an increase in the membrane fluidity to optimize photosynthetic activity under low
522 light conditions. Such physiological adaptation was found in seagrasses living along a depth
523 gradient (Beca-Carretero et al., 2019) and macroalgae in contrasting seasons (Schmid et al.,
524 2014). In late autumn 2017 g 2018, the decrease in desaturation indicated a reduced fluidity
525 and activity of photosynthetically active membranes (Quigg et al., 2006; Wacker et al., 2016).
526 This was associated with a decreased abundance of shoots and above-ground biomass. By
527 shedding leaves and shoots the plant further balances metabolic requirements and mobilize
528 energy from the carbohydrate reserves stored in the belowground tissue (Alcoverro et al.,
529 2001; Lee et al., 2007). During the winter, due to a sharp and continuous decrease in water
530 temperature, rapid desaturation of increasing lipids provided a cold resistance, as regularly
531 observed in algae and plants (Terrados and Lopezjimenez, 1996; Iveša et al., 2004; Upchurch,
532 2008).

533 In a healthy seagrass meadow, the oxygen generated by seagrass photosynthesis is
534 transported to belowground tissues to maintain an oxic microsphere around roots and
535 rhizomes, re-oxidize sulfide to non-toxic S^0 , thus preventing an invasion of H_2S into the plant
536 (Pedersen et al., 1998; Holmer et al, 2005). S^0 was found in the *C. nodosa* below-ground
537 tissue during the entire investigation period, as already observed in seagrasses living in
538 sulfidic sediments (Holmer and Hasler-Sheetal, 2014; Hasler-Sheetal and Holmer, 2015). The
539 relatively low accumulation of H_2S ($< 30 \mu M$) during the summer and early autumn 2017
540 indicated that H_2S was apparently rapidly recycled within the rooted area via re-oxidation by
541 O_2 to S^0 and/or removal by precipitation with iron compounds. Most of S^0 was found in oxic
542 layers or suboxic/anoxic boundaries, being in ranges typical for sulfidic coastal sediments
543 (Troelsen and Jørgensen, 1982; Panutrakul et al., 2001; Pjevac et al., 2014). The oxidation of

544 H₂S could occur spontaneously by chemical reaction with free oxygen or mediated by sulfide-
545 oxidizing bacteria surrounding or being attached to seagrass roots (Jørgensen, 1977; Cucio et
546 al., 2016; Ugarelli et al., 2017; Fahimipour et al., 2017). In November, due to the degradation
547 of organic matter and reduced oxygen production and leakage in the rooted zone caused by *C.*
548 *nodosa* senescence, the re-oxidation capacity of the sediment was greatly decreased. This
549 resulted in considerable accumulation of H₂S (> 100 µM) which extended up to the sediment
550 surface. During winter and early spring, H₂S production generally decreased, likely due to the
551 reduced activity of sulfate reducing prokaryotes at lower temperatures, and the sediment
552 gradually shifted towards a more oxidized state. H₂S detected even in within the oxic
553 sediment and in the rooted area in February 2018 could be attributed to the sediment
554 heterogeneity and the presence of reducing micro-niches where anaerobic metabolism could
555 occur regardless of surrounding redox conditions (Jørgensen, 1977; Frederiksen and Glud,
556 2006).

557 In April 2018, *C. nodosa* had been most probably exposed to increased siltation, due to an
558 increase in terrigenous input combined with resuspension of sediment provoking elevated
559 autotrophic growth. The intensive siltation is associated with the increased light attenuation,
560 both through the direct shading effect of suspended sediments and through the promotion of
561 phytoplankton and epiphyte growth by the associated increase in nutrients (Terrados et al.,
562 1998; Halun et al., 2002; Brodersen et al., 2015). Therefore, the increase in seawater turbidity
563 and considerable sediment re-deposition on the leaves might have severely impaired the light
564 availability and slowed down the plant's photosynthetic activity as indicates LA/ALA > 1 in
565 the above-ground tissue resulting from decreased conversion of LA to ALA (Harris and
566 James, 1965). When the minimum light requirements (~14% of incidence light) are not met,
567 *C. nodosa* intensely sheds leaves and shoots (Collier et al., 2012). Such light condition
568 apparently persisted until May 2018 and most likely prevented the re-establishment of
569 photosynthesis and *C. nodosa* continued to shed shoots and leaves. The reduced
570 photosynthesis and therefore O₂ transport from the leaves to the rhizome-root system
571 probably minimized root respiration. The maintenance of the oxic rhizosphere and the internal
572 O₂ partial pressure in the lacunae further depended mainly on the diffusion of O₂ from the
573 water column. From April to June 2018, O₂ in the bottom water drastically decreased. Due to
574 poor supply, O₂ content of the belowground tissue was too low to maintain the oxic

575 microenvironment and therefore, the plant tissues became potentially accessible to sulfide
576 intrusion (Pedersen et al., 2004).

577 At the same time, the sediment was enriched with fresh organic matter derived from
578 increased autotrophic biomass in bottom waters. In addition to the induction of the bloom,
579 strong sediment resuspension, most likely by aeration, stimulated the intense oxidation of H₂S
580 that started to produce in the rooted zone (up to 180 μM), due to increased activity of sulfate
581 reducing prokaryotes possibly triggered by the increase in temperature. An increase in S⁰
582 concentration that reached its maximum in the same layer suggests a simultaneous oxidation
583 of the produced H₂S. The sulfide oxidation probably caused oxygen depletion in the rooted
584 zone and anoxic zone extension up to the sediment subsurface. In May 2018, the excess of
585 organic matter accumulated in April 2018 was degraded. The concentrations of S⁰, detected
586 only in the suboxic layer, considerably decreased possibly by disproportionation or respiration
587 by members of the sulfate reducing bacteria (Pjevac et al., 2014).

588 During June and July 2018, a sudden and significant deterioration of *C. nodosa*
589 physiological condition was indicated by the further increase in LA/ALA ratio in the leaves
590 and overall saturation of decreasing lipids in above- and below-ground tissues. Additionally,
591 the loss of leaf tissue negatively impacted the photosynthetic carbon fixation and therefore
592 oxygen production, including the transport of oxygen to below-ground tissue (Lee and
593 Dunton, 1997; Lee et al., 2007). The below-ground tissue that was not supported by
594 photosynthetically derived oxygen became anoxic. Thus induced anaerobiosis most likely
595 caused a complete inhibition of the fatty acid desaturation chain (Harris and James, 1965) and
596 a permanent breakdown of photosynthesis leading to the final decay of the above-ground
597 biomass and considerable loss of below-ground biomass. As the bottom waters were
598 completely depleted in O₂ the whole plant was probably exposed to sulfides. H₂S inhibit
599 cytochrome c oxidase by binding to regulatory sites on the enzyme, reducing the rate of
600 cellular respiration and leading to the chemical asphyxiation (Nichols et al., 2013).

601 From June to August 2018, the decomposition of organic matter, encompassing the entire
602 sediment core, was intensified and accompanied by a large increase in H₂S concentrations (up
603 to 1200 μM). The degradation process involved rhizomes and roots, as suggested by the
604 apparent loss of belowground biomass. Such loss typically occurs in the first stage of plant
605 decay, the leaching phase (Trevathan-Tackett et al., 2017). Readily available, soluble
606 carbohydrates that largely contribute to the leachate mass (Vichkovitten and Holmer, 2004)

607 most probably supported the increase in prokaryotic abundance observed in June and July
608 2018. However, the significant decrease in prokaryotic abundance that coincided with a
609 maximum degradation of organic matter and H₂S production in August 2018 might indicate
610 that remaining compounds were not degradable by the sulfate reduction pathway (Arndt et al.,
611 2013) and needed the presence of prokaryotes specialized in the anaerobic degradation of
612 refractory compounds, including cellulose and lignin.

613 During September and October 2018, H₂S concentrations drastically decreased, and the
614 sediment was gradually enriched in fresh organic matter. Due to the combined effect of
615 freshened oxygenated water inflow and resuspension which gradually deepened the oxic
616 layer, re-oxidation of H₂S increased. Biogeochemical studies suggest that most sulfides (80 –
617 90 %) are eventually re-oxidized; 10 – 20 % are ultimately buried as complexes with iron (i.e.
618 FeS, FeS₂) or with organic matter after sulfurization (Jørgensen, 1977; 1982). H₂S scavenging
619 with iron and formation of iron sulfides might be more important in Saline Bay, since
620 terrestrial waters are washing out *terra rossa*, rich in Fe-oxides and oxyhydroxides (Durn,
621 2003). For this reason, sediment cores were most likely always black with sulfuric odor,
622 irrespective of H₂S concentrations or presence of vegetation.

623

624 5 Conclusions

625 Our results provide insights into the interaction of multiple stressors that have led to the
626 meadow decay, triggered in the sensitive recruitment phase of meadow growth. Even after the
627 improvement of the sediment conditions by the end of the summer 2018, *C. nodosa* was not
628 able to recolonize its previously occupied areas. This finding combined with a visible
629 alteration of the water column and sediment indicates a considerable loss of the *C. nodosa*
630 habitat. Further research is needed to examine the fate of Saline Bay meadows and an
631 eventual recolonization of the area.

632 Beyond seagrass itself, this loss had extensive consequences as it has endangered many
633 species that depend on seagrass for food, shelter and nursery. Given the lack of data on the
634 ecological and conservation status of the still numerous seagrass meadows along the northern
635 Adriatic coast, the identification and monitoring of the main pressures acting on them are
636 needed to protect such valuable habitats from degradation and extinction.

637

638 *Author contribution:* Conceptualization: MN, MK and GJH; Investigation: MK, PP, MM,
639 II, LJI, IF and MN; Formal analysis and Writing - original draft: MN; Writing – review &
640 editing: MK, GJH, PP, LJI, II, IF and MM.

641 *Competing interests:* The authors declare that they have no conflict of interest.

642 *Acknowledgements.* The financial support was provided by the Croatian Science Foundation
643 to MN (project IP-2016-06-7118, MICRO-SEAGRASS). We sincerely thank J. Jakovčević
644 and M. Buterer for nutrient and chlorophyll *a* determination, and A. Budiša and I. Haberle for
645 occasional help during separation and biometry of plant material.

646 **References**

- 647 Agostini, S., Pergent, G., and Marchand, B.: Growth and primary production of *Cymodocea*
648 *nodosa* in a coastal lagoon. *Aquat. Bot.*, 76, 185-193, 2003.
- 649 Alcoverro, T., Manzanera, M., and Romero J.: Annual metabolic carbon balance of the
650 seagrass *Posidonia oceanica*: the importance of carbohydrate reserves. *Mar. Ecol. Prog.*
651 *Ser.*, 211, 105-116, 2001.
- 652 Arndt, S., Jørgensen, B.B., LaRowe, D.E., Middelburg, J.J., Pancost, R.D., and Regnier, P.:
653 Quantifying the degradation of organic matter in marine sediments: A review and
654 synthesis. *Earth-Science Rev.*, 123, 53-86, 2013.
- 655 Beca-Carretero, P., Guihéneuf, F., Marín-Guirao, L., Bernardeau-Esteller, J., García-Muñoz,
656 R., Stengel, D.B., and Ruiz, J.M. Effects of an experimental heat wave on fatty acid
657 composition in two Mediterranean seagrass species. *Mar. Pollut. Bull.*, 134, 27-37, 2018.
- 658 Beca-Carretero, P., Guihéneuf, F., Winters, G., and Stengel, D.B.: Depth-induced adjustment
659 of fatty acid and pigment composition suggests high biochemical plasticity in the tropical
660 seagrass *Halophila stipulacea*. *Mar. Ecol. Prog. Ser.*, 608, 105-117, 2019.
- 661 Borum, J., Pedersen, O., Greve, T.M. Frankovich, T.A., Zieman, J.C., Fourqurean, J.W., and
662 Madden, C.J.: The potential role of plant oxygen and sulphide dynamics in die-off events
663 of the tropical seagrass, *Thalassia testudinum*. *J. Ecol.*, 93, 148-158, 2005.
- 664 Bourbonniere, R.A., and Meyers, P.A.: Sedimentary geolipid records of historical changes in
665 the watersheds and productivities of Lakes Ontario and Erie. *Limnol. Oceanogr.*, 41, 352-
666 359, 1996.
- 667 Brodersen, K.E., Lichtenberg, M., Paz, L-C., and Kühl, M.: Epiphyte-cover on seagrass
668 (*Zostera marina* L.) leaves impedes plant performance and radial O₂ loss from the bellow-
669 ground tissue. *Front. Mar. Sci.*, 2, 58 doi: 10.3389/fmars.201500058, 2015.
- 670 Cancemi, G., Buia, M.C., and Mazzella, L.: Structure and growth dynamics of *Cymodocea*
671 *nodosa* meadows. *Sci. Mar.*, 66: 365-373, 2002.
- 672 Canfield, D.E., Jørgensen, B.B., Fossing, H., Glud, R., Gundersen, J., Ramsing, N.B.,
673 Thamdrup, B., Hansen, J.W., Nielsen, L.P., and Hall, P.O.J.: Pathways of organic carbon
674 oxidation in three continental margin sediments. *Mar. Geol.*, 113, 27-40, 1993.
- 675 Capone, D.G., and Kiene, R.P.: Comparison of microbial dynamics in marine and freshwater
676 sediments: Contrasts in anaerobic carbon catabolism. *Limnol. Oceanogr.*, 33, 725-749,
677 1988.

678 Carlson, P.R., Yarbrow, L.A., and Barber, T.R.: Relationship of sediment sulfide to mortality of
679 *Thalassia testudinum*, Florida Bay. Bull. Mar. Sci., 54, 733-746, 1994.

680 Cebrian, J., Duarte, C.M., and Marbà, N.: Herbivory on the seagrass *Cymodocea nodosa*
681 (Ucria) Ascherson in contrasting Spanish Mediterranean habitats. J. Exp. Mar. Biol. Ecol.,
682 204, 103-111, 1996.

683 Cline, J.D.: Spectrophotometric determination of hydrogen sulfide in natural waters. Limnol.
684 Oceanogr., 14, 454-458, 1969.

685 Collier, C.J., Lavery, P.S., Masini, R.J., and Ralph, P.J.: Shade-induced response and recovery
686 of the seagrass *Posidonia sinuosa*. J. Exp. Mar. Biol. Ecol., 370, 89-103, 2009.

687 Collier, J.C., Waycott, M., and Giraldo Ospina, A.: Responses of four Indo-West Pacific
688 seagrass species to shading. Mar. Pollut. Bull., 65, 342-354, 2012.

689 Costa, M.M., Barrote, I., Silva, J., Olivé, I., Alexandre, A., Albano, S., and Santos, R.:
690 Epiphytes modulate *Posidonia oceanica* photosynthetic production, energetic balance,
691 antioxidant mechanisms, and oxidative damage. Front. Mar. Sci. 2:111, 2015.

692 Cranwell, P.A., Eglinton, G., and Robinson, N.: Lipids of aquatic organisms as potential
693 contributors to lacustrine sediments. Org. Geochem., 11, 513-527, 1987.

694 Cúcio, C., Engelen, A.H., Costa, R., and Muyzer, G.: Rhizosphere Microbiomes of European
695 Seagrasses Are Selected by the Plant, But Are Not Species Specific. Front. Microbiol., 7,
696 440. doi: 10.3389/fmicb.2016.00440, 2012.

697 Duarte, C.M., Kennedy, H., Marbà, N., Gacia, E., Fourqurean, J.W., Beggins, J., Barrón, C.,
698 Apostolaki, E.T.: Seagrass community metabolism: Assessing the capacity of seagrass
699 meadows for carbon burial: Current limitations and future strategies. Ocean Coast. Manag.,
700 83, 32-38, 2013.

701 Durn, G.: *Terra Rossa* in the Mediterranean Region: Parent Materials, Composition and
702 Origin. Geologia Croatica, 56, 83-100, 2003.

703 Epstein, S.S., and Rossel J.: Enumeration of sandy sediment bacteria: search for optimal
704 protocol. Mar. Ecol. Prog. Ser., 117, 289-298, 1995.

705 Fahimipour, A.K., Kardish, M.R., Lang, J.M., Green, J.L., Eisen, J.A., and Stachowicz, J.J.:
706 Global-Scale Structure of the Eelgrass Microbiome. Appl. Environ. Microbiol., 83,
707 e03391-16, 2017.

708 Folk, R.L.: The distinction between grain size and mineral composition in sedimentary-rock
709 nomenclature. J. Geol., 62, 344-359, 1954.

710 Frederiksen, M.S., Holmer, M., Pérez, M., Invers, O., Ruiz, J.M., and Knudsen, B.: Effect of
711 increased sediment sulfide concentrations on the composition of stable sulfur isotopes
712 ($\delta^{34}\text{S}$) and sulfur accumulation in the seagrasses *Zostera marina* and *Posidonia oceanica*.
713 J. Exp. Mar. Biol. Ecol., 358, 98-109, 2008.

714 Frederiksen, M.S., and Glud, R.N.: Oxygen dynamics in the rhizosphere of *Zostera marina*: A
715 two-dimensional planar optode study. Limnol. Oceanogr., 51, 1072-1083, 2006.

716 Gacia, E., and Duarte, C.M.: Sediment Retention by a Mediterranean *Posidonia oceanica*
717 Meadow: The Balance between Deposition and Resuspension. Estuar. Coast. Shelf. Sci.,
718 52, 505–514, 2001.

719 Gangi, A.F.: Permeability of unconsolidated sands and porous rocks. J. Geophys. Res. –Solid,
720 90, 3099-3104, 1985.

721 Gao, G., Clare, A.S., Chatzidimitriou, E., Rose, C., and Caldwell, G.: Effects of ocean
722 warming and acidification, combined with nutrient enrichment, on chemical composition
723 and functional properties of *Ulva rigida*. Food Chem., 258, 71-78, 2018.

724 Greve, T.M., Borum, J., and Pedersen, O.: Meristematic oxygen variability in eelgrass
725 (*Zostera marina*). Limnol. Oceanogr., 48, 210-216, 2003.

726 Halun, Z., Terrados, J., Borum, J., Kamp-Nielsen, J., Duarte, C.M., and Fortes, M.D.:
727 Experimental evaluation of the effects of siltation-derived changes in sediment conditions
728 on the Philippine seagrass *Cymodocea rotundata*. J. Exp. Mar. Biol. Ecol., 279, 73-87,
729 2002.

730 Harris, R.V., and James, A.T.: Linoleic and α -linolenic acid biosynthesis in plant leaves and a
731 green alga. Biochim. Biophys. Acta, 106, 456-464, 1965.

732 Hasler-Sheetal, H., and Holmer, M.: Sulfide intrusion and detoxification in the seagrass
733 *Zostera marina*. Plos One 10(6): e0129136, 2015.

734 Hendriks, I.E., Sintes, T., Bouma, T.J., and Duarte, C.M.: Experimental assessment and
735 modeling evaluation of the effects of the seagrass *Posidonia oceanica* on flow and particle
736 trapping. Mar. Ecol. Prog. Ser., 356, 163-173, 2008.

737 Holm-Hansen, O., Lorenzen, C. J., Holmes, R. W., and Strickland, J. D. H.: Fluorometric
738 determination of chlorophyll. J. Conseil., 301, 3-15, 1965.

739 Holmer, M., Duarte, C.M., Boschker, H.T.S., and Barrón, C.: Carbon cycling and bacterial
740 carbon sources in pristine and impacted Mediterranean seagrass sediments. Aquat. Microb.
741 Ecol., 36, 227-237, 2004.

742 Holmer, M., and Hasler-Sheetal, H.: Sulfide intrusion in seagrasses assessed by stable
743 isotopes- a synthesis of current results. *Front. Mar. Sci.*, doi: 10.3389/fmars.2014.00064,
744 2014.

745 Holmer, M., and Nielsen, S.L.: Sediment sulfur dynamics related to biomass-density pattern
746 in *Zostera marina* (eelgrass) beds. *Mar. Ecol. Prog. Ser.*, 146, 163-171, 1997.

747 Holmer, M., Frederiksen, M.S., and Møllegaard, H.: Sulfur accumulation in eelgrass (*Zostera*
748 *marina*) and effect of sulfur on eelgrass growth. *Aquat. Bot.*, 81, 367-379, 2005.

749 Holmer, M., Pedersen, O., and Ikejima, K.: Sulfur cycling and sulfide intrusion in mixed
750 Southeast Asian tropical seagrass meadows. *Bot. Mar.*, 49, 91-102, 2006.

751 Ivančić, I., Paliaga, P., Pfannkuchen, M., Đakovac, T., Najdek, M., Steiner, P., Korlević, M.,
752 Markovski, M., Baričević, A., Smodlaka Tanković, M., and Herndl, G.J.: Seasonal
753 variations in extracellular enzymatic activity in marine snow-associated microbial
754 communities and their impact on the surrounding water. *FEMS Microbiol. Ecol.*, 94,
755 fyi198, 2018.

756 Iveša, Lj., Blažina, M., and Najdek, M.: Seasonal variations in fatty acid composition of
757 *Caulerpa taxifolia* (M. Vahl.) C. Ag. in the northern Adriatic Sea (Malinska, Croatia). *Bot.*
758 *Mar.*, 47, 209-214, 2004.

759 Jørgensen, B.B.: The sulfur cycle of a coastal marine sediment (Limfjorden, Denmark).
760 *Limnol. Oceanogr.*, 22, 814-832, 1977.

761 Jørgensen, B.B.: Mineralization of organic matter in the sea bed - the role of sulphate
762 reduction. *Nature*, 296, 643-645, 1982.

763 Koch, M.S., and Erskine, J.M.: Sulfide as a Phytotoxin to the Tropical Seagrass *Thalassia*
764 *testudinum*: Interactions with Light, Salinity and Temperature. *J. Exp. Mar. Biol. Ecol.*,
765 266, 81-95, 2001.

766 Krause-Jensen, D., Carstensen, J., Nielsen, S.L., Dalsgaard, T., Christensen, P.B., Fossing, H.,
767 and Rasmussen, M.B.: Sea bottom characteristics affect depth limits of eelgrass *Zostera*
768 *marina*. *Mar. Ecol. Prog. Ser.*, 425, 91-102, 2011.

769 Lee, K-S., and Dunton, K.H.: Diurnal changes in pore water sulfide concentrations in the
770 seagrass *Thalassia testudinum* beds: the effects of seagrasses on sulfide dynamics. *J. Exp.*
771 *Mar. Biol. Ecol.*, 255, 201-214, 2000.

772 Lee, K-S., Park, S.R., and Kim, Y.K.: Effects of irradiance, temperature, and nutrients on
773 growth dynamics of seagrasses: A review. *J. Exp. Mar. Biol. Ecol.*, 350, 144-175, 2007.

774 Marbà, N., and Duarte, C.M.: Growth and sediment space occupation by seagrass *Cymodocea*
775 *nodosa* roots. Mar. Ecol. Prog. Ser., 224, 291-298, 2001.

776 Mascaró, O., Valdemarsen, T., Holmer, M., Pérez, M., and Romero, J.: Experimental
777 manipulation of sediment organic content and water column aeration reduces *Zostera*
778 *marina* (eelgrass) growth and survival. J. Exp. Mar. Biol. Ecol., 373, 26-34, 2009.

779 Micromeritics: SediGraph 5100 particle size analysis system operator' manual. Micromeritics
780 Instrument Corporation, Norcross, 2002.

781 Moeslund, L., Thamdrup, B., and Jørgensen, B.B.: Sulfur and iron cycling in a coastal
782 sediment—radiotracer studies and seasonal dynamics. Biogeochemistry, 27, 129-152,
783 1994.

784 Nicholls, P., Marshall, D.C., Cooper, C.E., and Wilson, M.T.: Sulfide inhibition of and
785 metabolism by cytochrome c oxidase. Biochem. Soc. Transact., 41, 1312-1316, 2013.

786 Orlando-Bonaca, M., Francé, J., Mavrič, B., Grego, M., Lipej, L., Flander Putrle, V., Šiško,
787 M., and Falace, A.: A new index (MediSkew) for the assessment of the *Cymodocea nodosa*
788 (Ucria) Ascherson meadow's status. Mar. Environ. Res., 110, 132-141, 2015.

789 Orlando-Bonaca, M., Francé, J., Mavrič, B., and Lipej, L.: Impact of the Port of Koper on
790 *Cymodocea nodosa* meadow. Annales, 29, 187-194, 2019.

791 Orth, R.J., Carruthers, T.J.B., Dennison, W.C., Duarte, C.M., Fourqurean, J.W., Heck Jr.,
792 K.L., Hughes, A.R., Kendrick, G.A., Kenworthy, E.J., Olyarnik, S., Short, F.T., Waycott,
793 M., and Williams, S.L.: A Global Crisis for Seagrass Ecosystems. BioScience, 56, 987-
794 996, 2006.

795 Panutrakul, S., Monteny, F., and Baeyens, W.: Seasonal Variations in Sediment Sulfur
796 Cycling in the Ballastplaat Mudflat, Belgium. Estuaries 24, 257-265, 2001.

797 Pedersen, M.F., Duarte, C.M., and Cebrián, J.: Rates of changes in organic matter and nutrient
798 stocks during seagrass *Cymodocea nodosa* colonization and stand development. Mar. Ecol.
799 Prog. Ser., 159, 29-36, 1997.

800 Pedersen, O., Borum, J., Duarte, C.M., and Fortes, M.D.: Oxygen dynamics in the rhizosphere
801 of *Cymodocea rotundata*. Mar. Ecol. Prog. Ser., 169, 283-288, 1988.

802 Pedersen, O., Binzer, T., and Borum, J.: Sulphide intrusion in eelgrass (*Zostera marina* L.).
803 Plant Cell Environ., 27, 595-602, 2004.

804 Peduzzi, P., and Herndl, G.J.: Decomposition and significance of seagrass litter (*Cymodocea*
805 *nodosa*) for the microbial food web in coastal waters (Gulf of Trieste, Northern Adriatic
806 Sea). *Mar. Ecol. Prog. Ser.*, 71, 163-174, 1991.

807 Pérez, M., Invers, O., Ruiz Fernandez, J.M., Frederiksen, M., and Holmer, M.: Physiological
808 responses of the seagrass *Posidonia oceanica* to elevated organic matter content in
809 sediments: An experimental assessment. *J. Exp. Mar. Biol. Ecol.*, 344,149-160, 2007.

810 Pirini, M., Manuzzi, M.P., Pagliarani, A., Trombetti, F., Borgatti, A.R., and Ventrella, V.:
811 Changes in fatty acid composition of *Mytilus galloprovincialis* (Lmk) fed on microalgal
812 and wheat germ diets. *Comp. Biochem. Physiol. B*, 147, 616-626, 2007.

813 Pjevac, P., Kamyshny Jr., A., Dyksma, S., and Mussmann, M.: Microbial consumption of
814 zero-valence sulfur in marine benthic habitats. *Environ. Microbiol.*, 16, 3416-3430, 2014.

815 Porter, K.G., and Feig, Y.S.: The use of DAPI for identification and counting aquatic
816 microflora. *Limnol. Oceanogr.*, 25, 943-984, 1980.

817 Quigg, A., Kevekordes, K., Raven, J., and Beardall, J.: Limitations on microalgal growth at
818 very low photon fluency rates: the role of energy slippage. *Photosynth. Res.*, 88, 299-310,
819 2006.

820 Rogowska, J., Sychowska, J., Cieszynska-Semenowicz, M., and Wolska, L.: Elemental sulfur
821 in sediments: analytical problems. *Environ. Sci. Pollut. Res.*, 23, 24871-24879, 2016.

822 Samper-Villarreal, J., Lovelock, C.E., Saunders, M.I., Roelfsema, C., and Mumby, P.J.:
823 Organic carbon in seagrass sediment is influenced by seagrass canopy complexity,
824 turbidity, wave height, and water depth. *Limnol. Oceanogr.*, 61, 938-952, 2016.

825 Sand-Jensen, K., Pedersen, O., Binzer, T., and Borum, J.: Contrasting Oxygen Dynamics in
826 the Freshwater Isoetid *Lobelia dortmanna* and the Marine Seagrass *Zostera marina*. *Ann.*
827 *Bot.*, 96, 613-623, 2005.

828 Schmid, M., Guihéneuf, F., and Stengel, D.B.: Fatty acid contents and profiles of 16
829 macroalgae collected from the Irish Coast at two seasons. *J. Appl. Phycol.*, 26, 451-463,
830 2014.

831 Short, F.T., Polidoro, B., Livingstone, S.R., Carpenter, K.E., Bandeira, S., Bujang, J.S.,
832 Calumpong, H.P., Carruthers, T.J.B., Coles, R.G., Dennison, W.C., Erftemeijer, P.L.A.,
833 Fortes, M.D., Freeman, A.S., Jagtap, T.G., Kamal, A.M., Kendrick, G.A., Kenworthy,
834 W.J., La Nafie, Y.A., Nasution, I.M., Orth, R.J., Prathep, A., Sanciangco, J.C., van

835 Tussenbroek, B., and Vergara, S.G.: Extinction risk assessment of the world's seagrass
836 species. *Biol. Conserv.*, 144, 1961-1971, 2011.

837 Sousa, A.I., Calado, R., Cleary, D.F.R., Nunes, C., Coimbra, M.A., Serôdio, J., and Lillebø,
838 A.I.: Effect of spatio-temporal shifts in salinity combined with other environmental
839 variables on the ecological processes provided by *Zostera noltii* meadows. *Sci. Rep.*, 7,
840 1336, 2017.

841 Strickland, J.D.H., and Parsons, T.R.: A practical handbook of seawater analysis. *Bull. Fish.*
842 *Res. Board. Can.*, 167,1-310, 1972.

843 Terrados, J., and Lopez-Jimenez, J.A.: Fatty acid composition and chilling resistance in the
844 green alga *Caulerpa prolifera* (Forsskal) Lamouroux (Chlorophyta, Caulerpales). *Biochem.*
845 *Molecul. Biol. Internatl.*, 39, 863-869, 1996.

846 Terrados, J., Duarte, C.M., Fortes, M.D., Borum, J., Agawin, N.S.R., Bach, S., Thampanya,
847 U., Kamp-Nielsen, L., Kenworthy, W.J., Geertz-Hansen, O., and Vermaat, J.: Changes in
848 Community Structure and Biomass of Seagrass Communities along Gradients of Siltation
849 in SE Asia. *Estuar. Coast. Shelf Sci.*, 46, 757-768, 1998.

850 Terrados, J., and Ros, J.D.: Growth and primary production of *Cymodocea nodosa* (Ucria)
851 Ascherson in a Mediterranean coastal lagoon: the Mar Menor (SE Spain). *Aquat. Bot.*, 43,
852 63-74, 1992.

853 Trevathan-Tackett, S.M., Seymour, J.R., Nielsen, D.A., Macreadie, P.I., Jeffries, T.C.,
854 Sanderman, J., Baldock, J., Howes, J.M., Steven, A.D.L., and Ralph, P.J.: Sediment anoxia
855 limits microbial-driven seagrass carbon remineralization under warming conditions. *FEMS*
856 *Microbiol. Ecol.*, 93,fix033, 2017.

857 Troelsen, H., and Jørgensen, B.B.: Seasonal dynamics of elemental sulfur in two coastal
858 sediments. *Estuar. Coast. Shelf Sci.*, 15, 255-266, 1982.

859 Tuya, F., Martín, J.A., and Luque, A.: Impact of a marina construction on seagrass bed at
860 Lanzarote (Canary Islands). *J. Coast. Conserv.*, 8, 157-162, 2002.

861 Tuya, F., Ribeiro-Leite, L., Arto-Cuesta, N., Coca, J., Haroun, R., and Espino, F.: Decadal
862 changes in the structure of *Cymodocea nodosa* seagrass meadows: Natural vs. human
863 influences. *Estuar. Coast. Shelf Sci.*, 137, 41-49 (2014).

864 Ugarelli, K., Chakrabarti, S., Laas, P., and Stingl, U.: The seagrass holobiont and its
865 microbiome. *Microorganisms* 5, 81, 2017.

866 Upchurch, R.G.: Fatty acid unsaturation, mobilization, and regulation in the response of plants
867 to stress. *Biotechnol. Lett.*, 30, 967-977, 2008.

868 Valentine, J.F., and Duffy, J.E.: The central role of grazing in seagrass ecology. In:
869 *Seagrasses: Biology, Ecology and Conservation*, Springer, Netherlands, pp 431-501, 2006.

870 Vaquer-Sunyer, R., and Duarte, C.M.: Thresholds of hypoxia for marine biodiversity. *PNAS*,
871 105, 15452-15457, 2008.

872 Vaquer-Sunyer, R., and Duarte, C.M.: Sulfide exposure accelerates hypoxia-driven mortality.
873 *Limnol. Oceanogr.*, 55, 1075-1082, 2010.

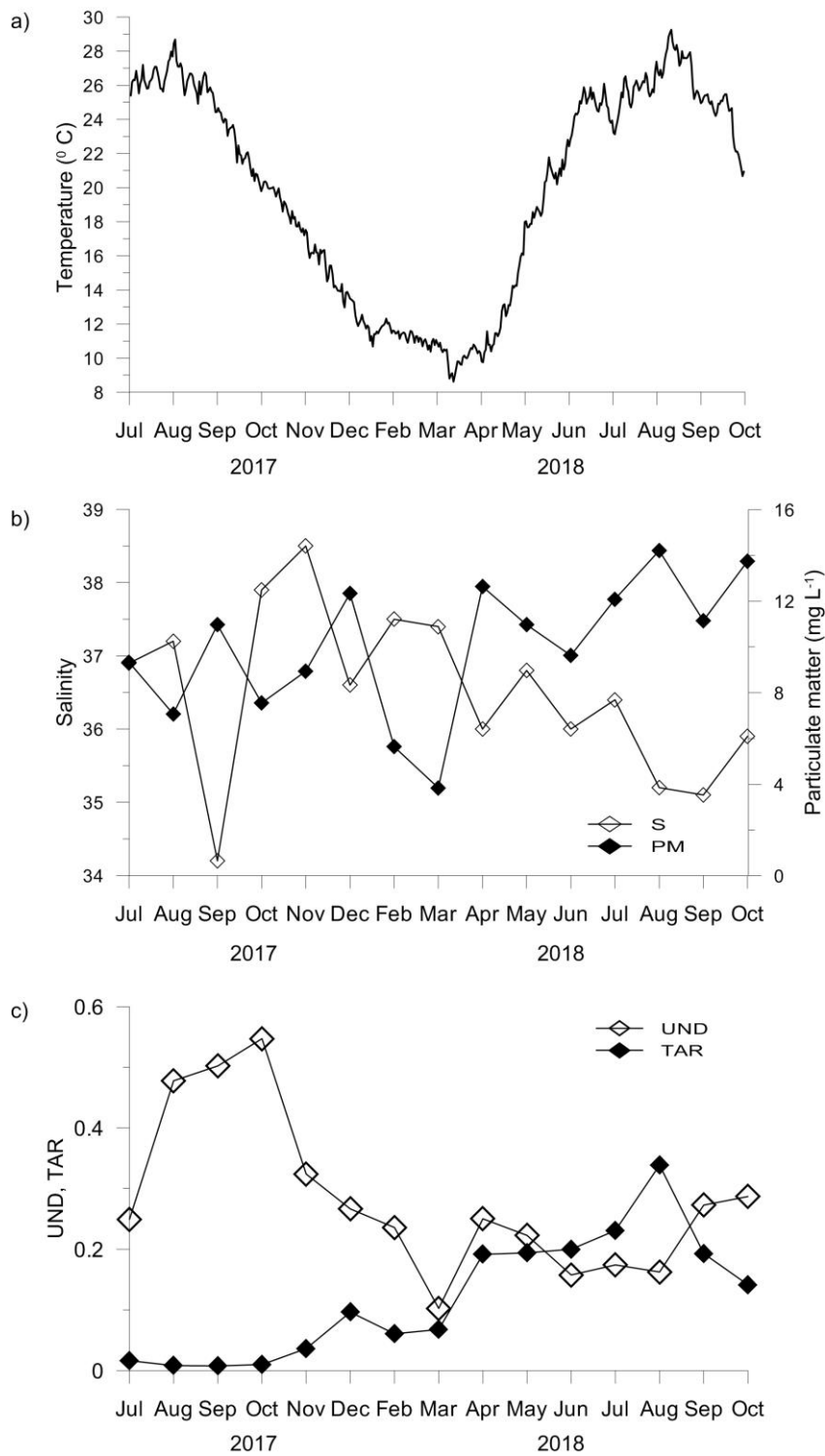
874 Viso, A.C., Pesando, D., Bernard, P., and Marty, J.C.: Lipid components of the Mediterranean
875 seagrass *Posidonia oceanica*. *Mar. Pollut. Bull.*, 34, 381-387, 1993.

876 Vichkovitten, T., and Holmer, M.: Contribution of plant carbohydrates to sedimentary carbon
877 mineralization. *Org. Geochem.*, 35, 1053-1066, 2004.

878 Wacker, A., Piepho, M., Harwood, J.L., Guschina, I.A., and Arts, M.T.: Light-induced
879 changes in fatty acid profiles of specific lipid classes in several freshwater phytoplankton
880 species. *Front. Plant Sci.*, 7, 264, 2016.

881 Widdows, J., Pope, N.D., Brinsley, M.D., Asmus, H., and Asmus, R.M.: Effects of seagrass
882 beds (*Zostera noltii* and *Z. marina*) on near-bed hydrodynamics and sediment
883 resuspension. *Mar. Ecol. Prog. Ser.*, 358, 125-136, 2008.

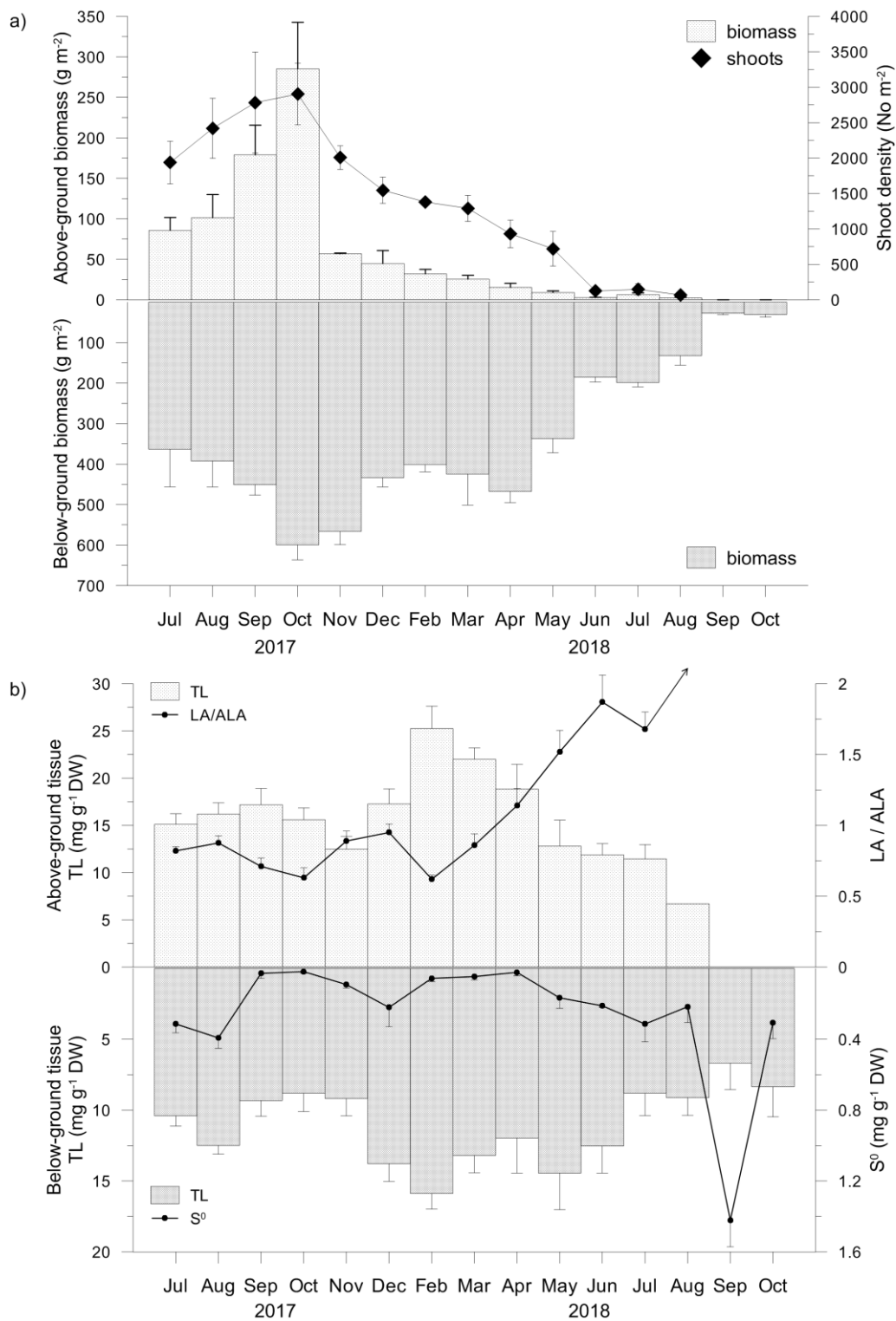
884 Zavodnik, N., Travizi, A., and De Rosa, S.: Seasonal variations in the rate of photosynthetic
885 activity and chemical composition of the seagrass *Cymodocea nodosa* (Ucr.) Asch. *Sci.*
886 *Mar.*, 62, 301-309, 1998.



887

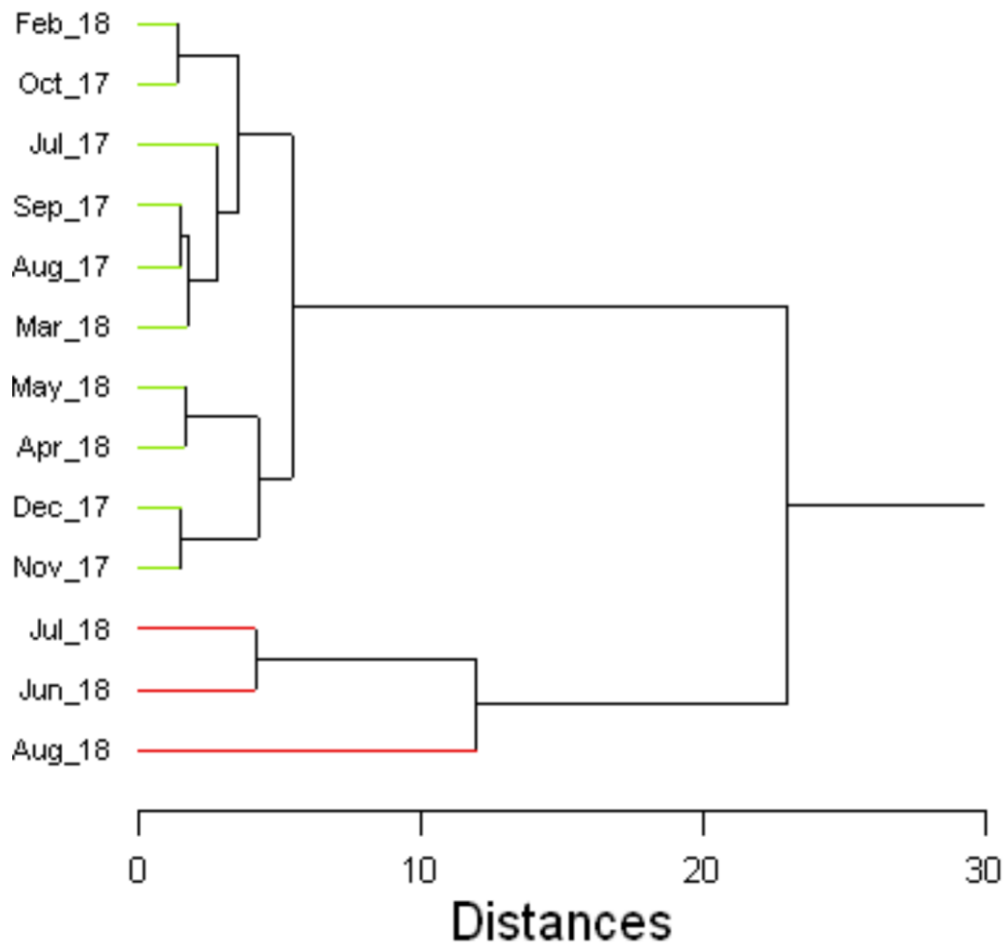
888

889 Figure 1. Temperature (a); salinity (b), particulate matter concentration (b); unsaturation
 890 degree (UND) and terrestrial to aquatic ratio (TAR) of the particulate lipid matter (c) in
 891 seawater.



892

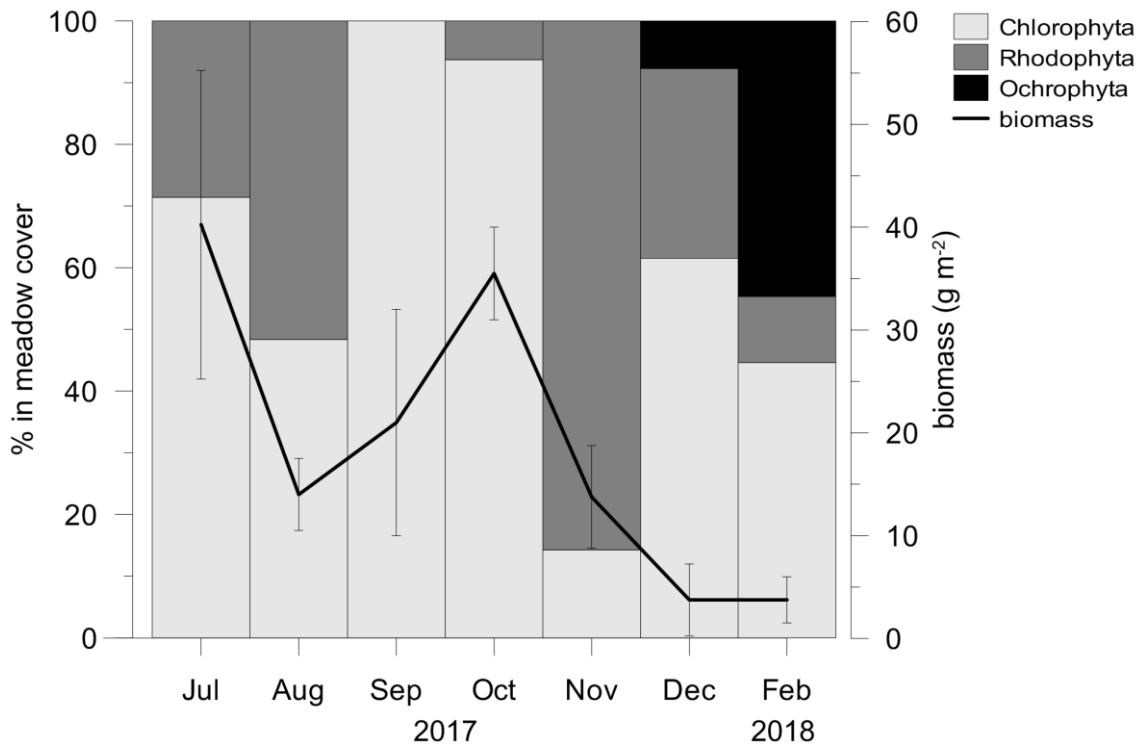
893 Figure 2. Above- and below-ground tissue biomasses and shoot density (a), total lipid
 894 concentrations (TL) and linoleic to α -linolenic fatty acids ratios (LA/ALA, an arrow indicates
 895 an infinite value) in above-ground tissue and TL and approximated concentrations of
 896 elemental sulfur (S⁰) in below-ground tissue (b).



897

898 Figure 3. Cluster analysis dendrogram of fatty acid composition of *C. nodosa* leaves.

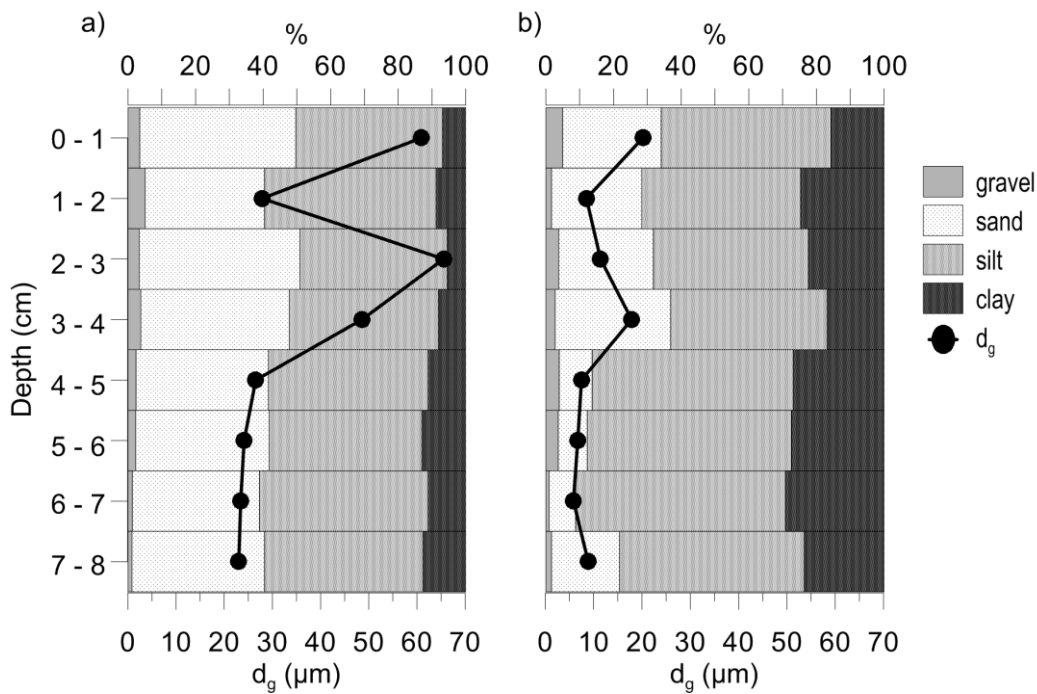
899 Summary statistics is given in Table S3.



900

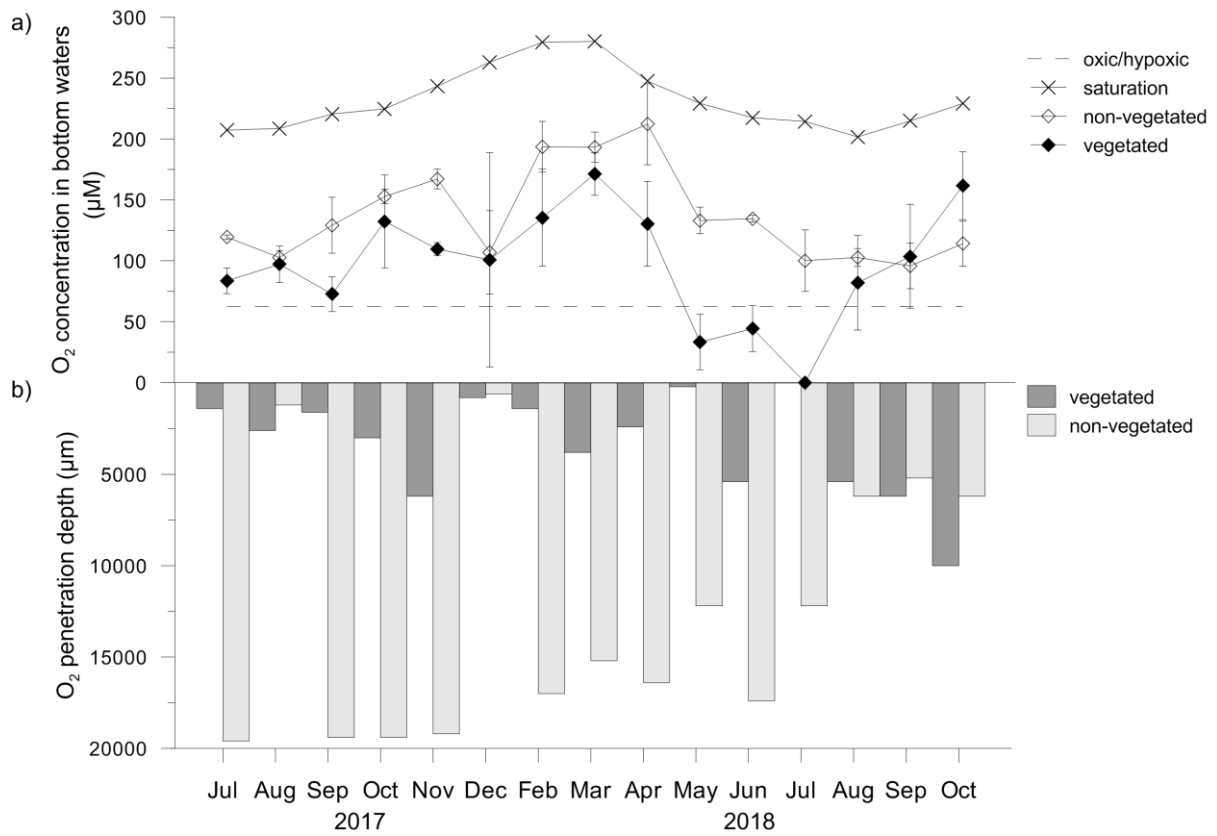
901 Figure 4. The contribution of macroalgal phyla in a meadow cover and total macroalgal
 902 biomass. After February 2018 macroalgae were no longer present in the *C. nodosa* meadow.

903



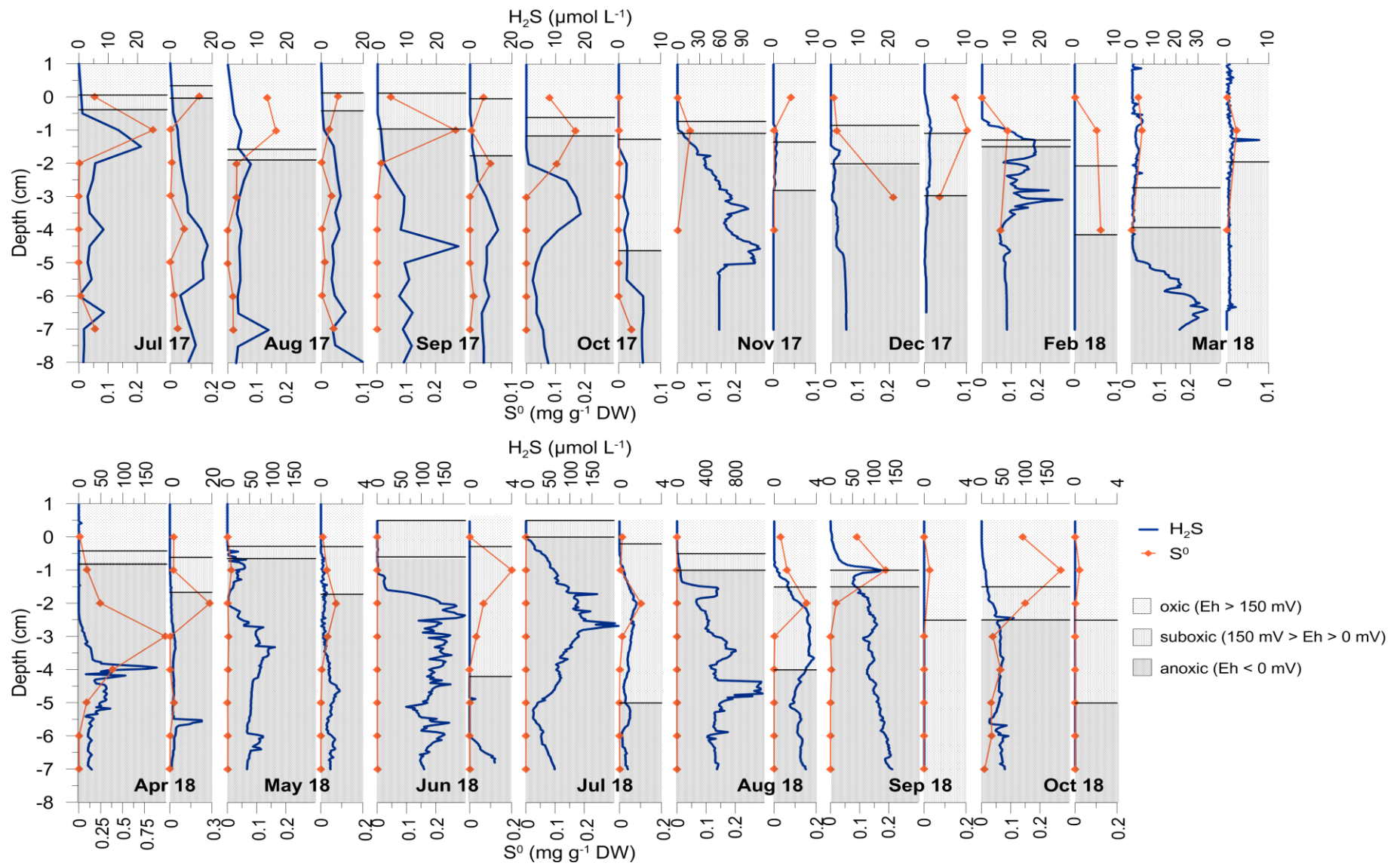
904

905 Figure 5. Granulometric composition and median grain size (d_g) of vegetated (a) and non-
 906 vegetated sediment (b).



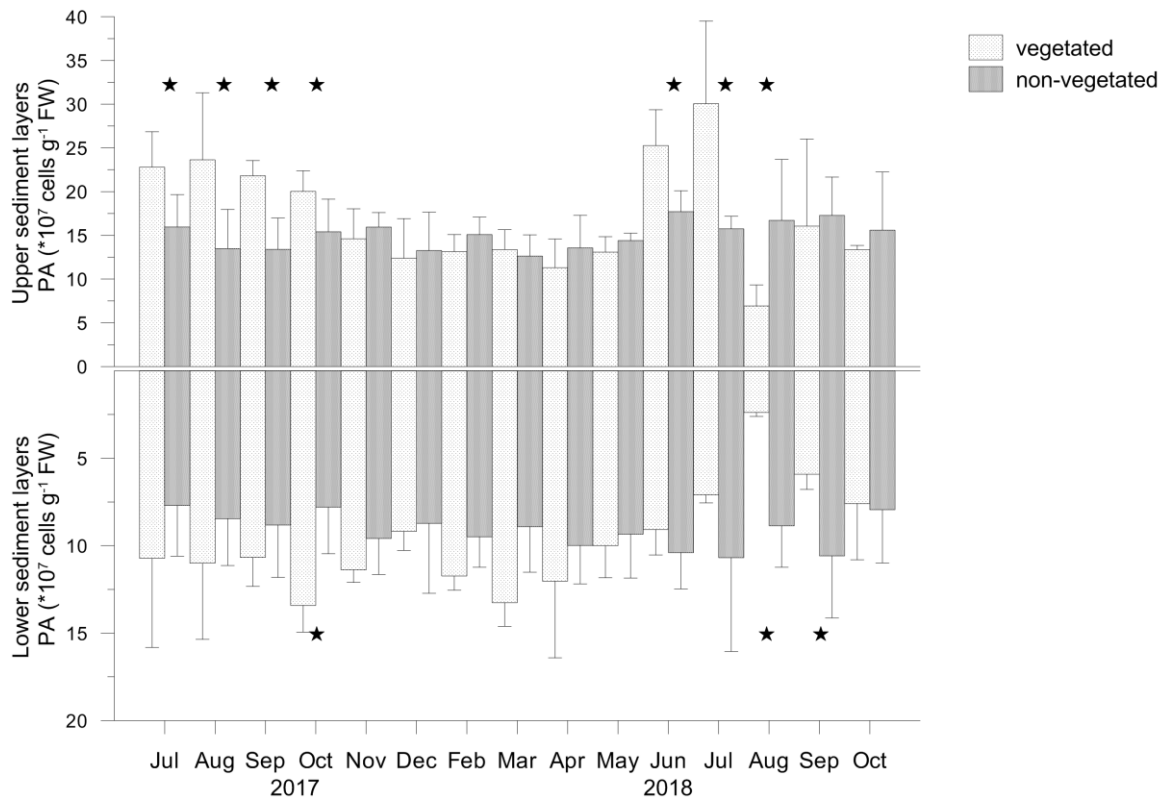
907

908 Figure 6. Oxygen concentrations (O₂) in bottom waters (a) and O₂ penetration depths (b)
 909 above and in vegetated and non-vegetated sediment, respectively. O₂ at the saturation level
 910 was calculated according to the temperature and salinity measured in seawater at the sampling
 911 dates; O₂ at the hypoxic frontier (~ 62.5 µM) was taken from Vaquer-Sanyer and Duarte
 912 (2008).



913

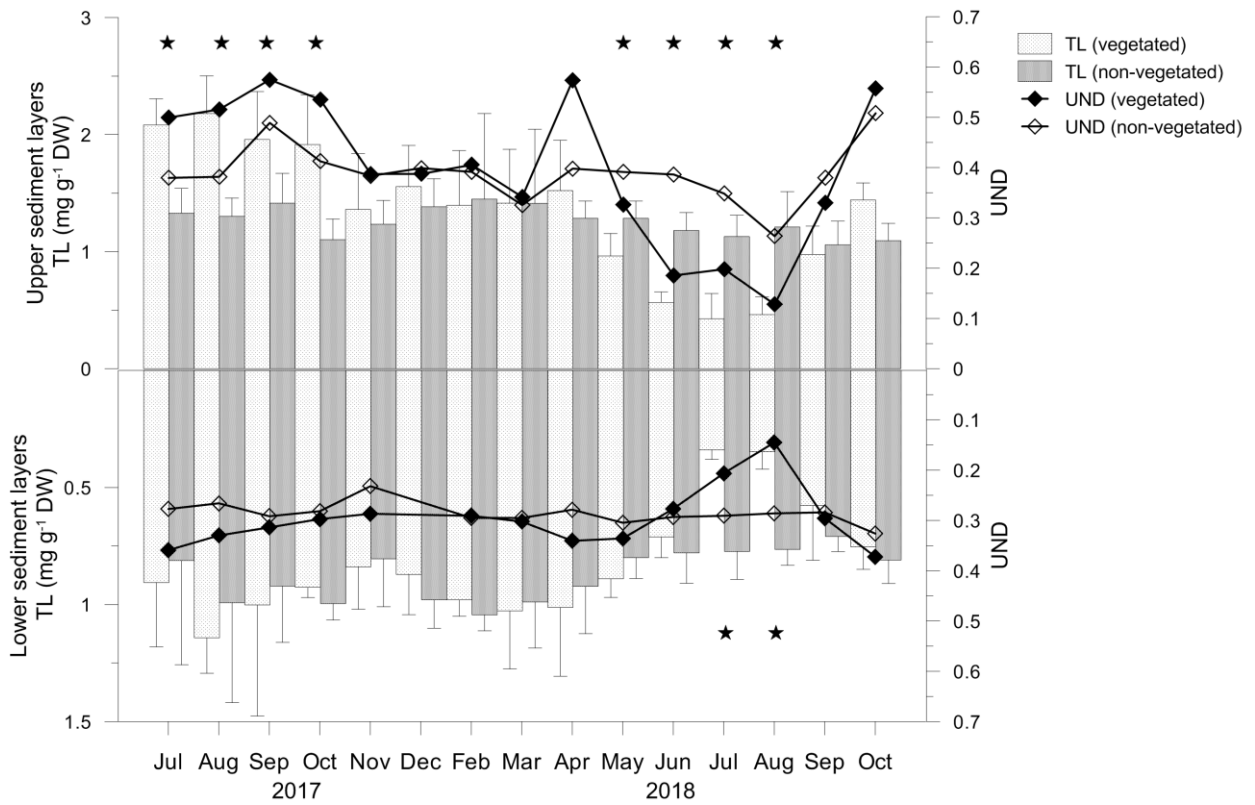
914 Figure 7. Depth profiles of H_2S and S^0 concentrations in vegetated and non-vegetated sediment (adjacent narrow graphs). The redox potential
 915 (Eh) in both sediments is shown as areas corresponding to oxic ($Eh > 150$ mV), suboxic ($150 > Eh > 0$ mV) and anoxic ($Eh < 0$ mV) conditions.



916

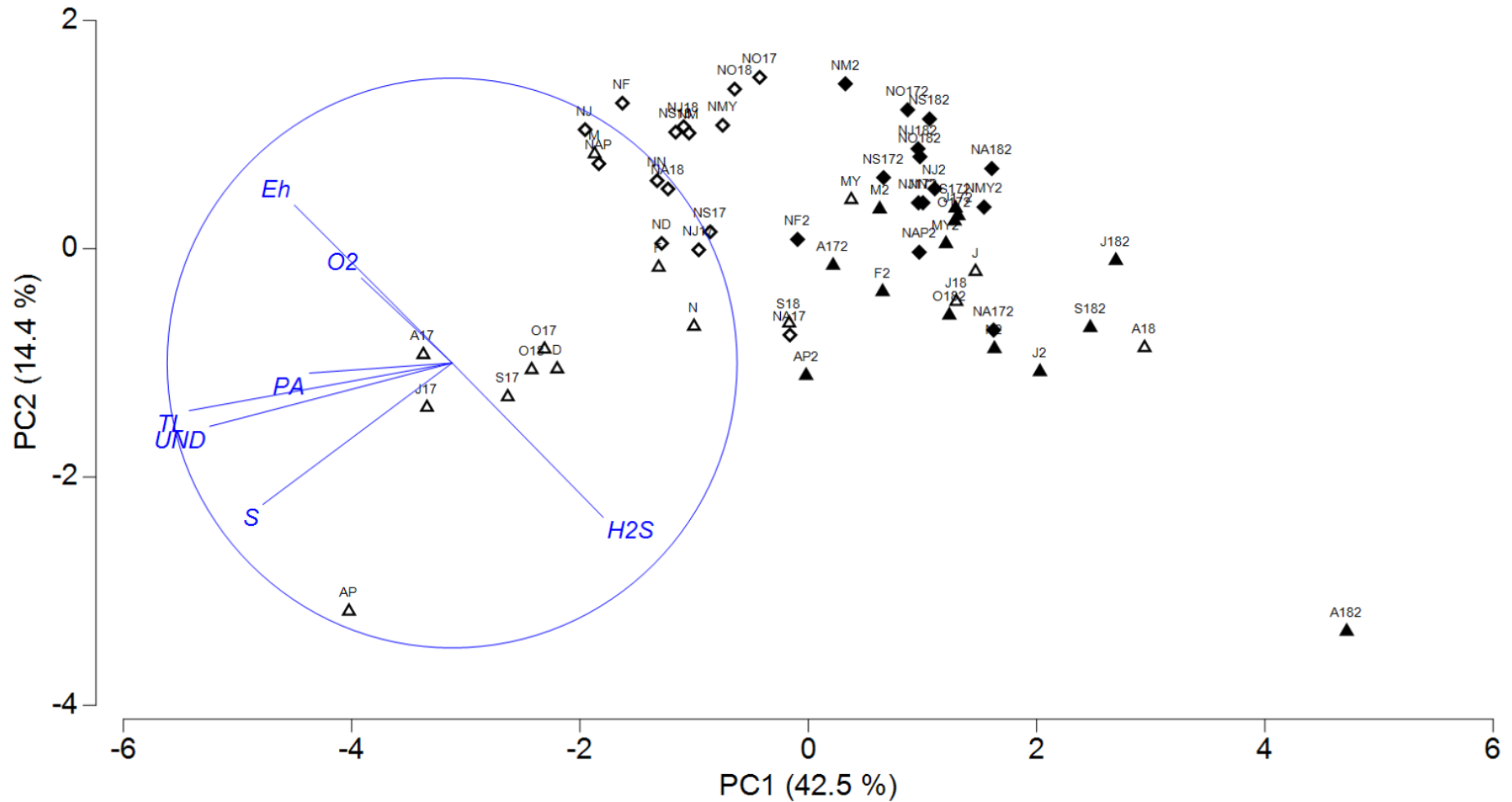
917 Figure 8. Prokaryotic abundance (PA) in the upper (0 - 4 cm) and lower (5 - 8 cm) layers of
 918 vegetated and non-vegetated sediments; significant differences in PA between the sediments
 919 are indicated by asterisks.

920



921

922 Figure 9. Total lipid concentrations (TL) and unsaturation degree (UND) in the upper (0 - 4
 923 cm) and lower (5 - 8 cm) layers of vegetated and non-vegetated sediments. Significant
 924 differences in TL between the sediments are indicated by asterisks.



926

927 Figure 10. PCA plot of redox potential (Eh), oxygen (O₂), hydrogen sulfide (H₂S), sulfur (S), total lipids (TL) and prokaryotes (PA)
 928 concentrations and unsaturation degree (UND) in the upper (0 – 4 cm; ▲, ◇) and lower (5 – 7 cm; ▲, ◆) layers of vegetated and non-vegetated
 929 sediments, respectively. Projections of variables are given in circle